Quadrupole moments of *sd*-shell nuclei

M. Carchidi and B. H. Wildenthal
Department of Physics and Atmospheric Science, Drexel University, Philadelphia, Pennsylvania 19104

B. A. Brown
National Superconducting Cyclotron Laboratory, Michigan State University, East Lansing, Michigan 48824
(Received 7 August 1986)

Shell-model calculations are presented for electric quadrupole moments of $A=17-39$ nuclei. The shell-model wave functions, which span the complete $0d_{5/2}$-$1s_{1/2}$-$0d_{3/2}$ model space in all instances, are obtained by diagonalizing an *sd*-shell Hamiltonian which consists of a fixed single-particle energy spectrum and a single set of two-body matrix elements scaled as a function of the mass number A. Results obtained with harmonic oscillator and Saxon-Woods single-particle radial wave functions and matched effective-charge models are presented for ground states of odd-even and doubly odd nuclei and for $J^{\pi}=2^{+}$ first-excited states of doubly even *sd*-shell nuclei.

I. INTRODUCTION

Static electric quadrupole moments of nuclear states provide fundamental information about nuclear deformations.[1] Their variations in sign and magnitude as a function of the mass and charge numbers A and Z are sensitive manifestations of the many-particle structures of the nuclear wave functions. To account for the complete range of quadrupole moments within a major shell is a thorough and comprehensive test of any theory for the structure of the relevant nuclei. In the *sd* shell, measurements of quadrupole moments have been carried out for almost all mass numbers and a complex sequence of structural transitions thereby mapped out. It is a fundamental challenge for a microscopic theory such as the shell model to account for the nuclear shape features reflected by these data.

Previous comprehensive analyses of $A=17-39$ quadrupole moments with shell-model wave functions[2-5] relied on calculations which incorporated different model-space truncations, different effective charges, and different model Hamiltonians for different portions of the mass range. These discontinuities and inconsistencies in earlier calculations made it difficult to distinguish systematic nuclear structure effects in the results from the inadvertent consequences of changes in the scope of the configuration space or of the specification of the effective interaction.

The predictions presented here surmount these earlier deficiencies. The present shell-model calculations[6] are internally consistent in that the models spaces uniformly span the complete $0d_{5/2}$-$1s_{1/2}$-$0d_{3/2}$ configuration space, in that every state is calculated from a model Hamiltonian generated from the same set of two-body matrix elements and single-particle energies, in that the effective charges used in the model $E2$ operator are independent of state and mass, and in that the single-particle radial wave functions are parametrized as functions of the mass in systematic ways.

The multiparticle wave functions[6] used in this study have been shown to yield predictions which agree well with experimental data on level energies,[6] single-nucleon transfer,[6] and Gamow-Teller/magnetic dipole phenomena.[7,8] The present comparisons of their predictions for electric quadrupole moments with experimental data provide tests of quite different properties of the wave functions, namely their shape-collective features. These comparisons can also provide information about the appropriate formulation of the effective charge of the model $E2$ operator and about the optimum prescription for the single-particle radial wave functions. Such features of the wave functions of Ref. 6 have been studied[9] in another context by a comparison of measured and predicted inelastic electron scattering form factors.

II. THEORY

A. General structure of multiparticle shell-model matrix elements

In this study we make the conventional assumption of the impulse approximation, namely, that the operator mediating electric quadrupole observables of a many-body nuclear state $|NJTT_z\rangle$ can be represented as a sum of one-body operators. A one-body operator O in the nuclear shell model can be represented in the second quantized formulation as[10]

$$O=\sum_{k=1}^{A} O_k=\sum_{\substack{\rho,\rho' \\ m,m'}} \langle \rho m \mid O \mid \rho' m' \rangle a^{\dagger}_{\rho m} a_{\rho' m'} , \qquad (1)$$

where the first summation runs over all nucleons, the second summation runs over all active single-particle states $|\rho m\rangle = |nljmtt_z\rangle$ in the shell-model basis space, and $a^{\dagger}_{\rho m}$ and $a_{\rho m}$ are the single-particle creation and annihilation operators, respectively, for these states. If the operator O is a spherical tensor of rank L in coordinate space, $O=O(L,M)$, then the Wigner-Eckart theorem in the form

$$\langle \rho m \mid O(L,M) \mid \rho' m' \rangle = (-1)^{j'-m'} \frac{\langle jmj'-m' \mid LM \rangle}{\sqrt{2L+1}} \times \langle \rho || O(L) || \rho' \rangle \quad (2)$$

can be used to factor out all m, m', and M dependence and reduce Eq. (1) to

$$O(L) = \sum_{\rho,\rho'} \langle \rho || O(L) || \rho' \rangle \frac{[a_\rho^\dagger \times \tilde{a}_{\rho'}]^L}{\sqrt{2L+1}} . \quad (3)$$

In Eq. (3) we have converted to the spherical tensor, $\tilde{a}_{\rho m} = (-1)^{\rho+m} a_{\rho -m}$ and have already performed the sum over all coordinate magnetic substates in the coupling

$$[a_\rho^\dagger \times \tilde{a}_{\rho'}]^L = \sum_{m,m'} \langle jmj'm' \mid LM \rangle a_{\rho m}^\dagger \tilde{a}_{\rho' m'} . \quad (4)$$

The reduced multiparticle matrix element of the one-body operator, $\langle NJTT_z || O(L) || NJTT_z \rangle$, may then be expressed as

$$\langle NJTT_z || O(L) || NJTT_z \rangle = \sum_{\rho,\rho'} \langle \rho || O(L) || \rho' \rangle D^{NJTT_z}(L,\rho,\rho') , \quad (5)$$

where $\langle \rho || O(L) || \rho' \rangle$ are single-particle matrix elements and

$$D^{NJTT_z}(L,\rho,\rho') = \frac{\langle NJTT_z || [a_\rho^\dagger \times \tilde{a}_{\rho'}]^L || NJTT_z \rangle}{\sqrt{2L+1}} \quad (6)$$

are one-body-transition densities. The values of the $D^{NJTT_z}(L,\rho,\rho')$ are determined by the appropriate algebraic operations on the model wave functions. They were thus completely determined by the diagonalizations of the Schrödinger equation $H \mid NJT \rangle = E \mid NJT \rangle$ which yielded the wave functions and energies of Ref. 6. The values of these one-body-transition densities for the states of interest in this study are listed in Table I.

B. Electric quadrupole operator and moment

The electric multipole operator is defined by

$$O(E,LM)_k = e_k r_k^L Y_{LM}(\hat{r}_k) , \quad (7)$$

and the definition of the total electric quadrupole moment in a state $\mid NJ(J_z=J)TT_z \rangle$ is[10]

$$Q = \sqrt{16\pi/5} \langle NJ(J_z=J)TT_z \mid \sum_{k=1}^{A} O(E;L=2,M=0)_k \mid NJ(J_z=J)TT_z \rangle , \quad (8a)$$

which, with the Wigner-Eckart theorem, can be written as

$$Q = \sqrt{16\pi/5} \begin{bmatrix} J & 2 & J \\ -J & 0 & J \end{bmatrix} \langle NJTT_z || \sum_{k=1}^{A} O(E2)_k || NJTT_z \rangle . \quad (8b)$$

Here [ ] represents the $3j$ symbol for the angular momentum factor, the value of which is given by

$$\begin{bmatrix} J & 2 & J \\ -J & 0 & J \end{bmatrix} = \left[\frac{J(2J-1)}{(2J+1)(J+1)(2J+3)} \right]^{1/2} .$$

It is useful to separate the proton and neutron contributions to the quadrupole matrix element and factor out the charge e_k and write

$$Q = \sqrt{16\pi/5} \begin{bmatrix} J & 2 & J \\ -J & 0 & J \end{bmatrix} \left[\langle NJTT_z || \sum_{\text{protons}} O(E2)_p || NJTT_z \rangle + \sum_{\text{neutrons}} \langle NJTT_z || O(E2)_n || NJTT_z \rangle \right] \quad (8c)$$

or

$$Q = \sqrt{16\pi/5} \begin{bmatrix} J & 2 & J \\ -J & 0 & J \end{bmatrix} [e_p A(E2)_p + e_n A(E2)_n] , \quad (8d)$$

where $A(E2)_{p/n}$ represents the $E2$ matrix elements,

$$A(E2)_{p/n} = \sum_{p/n} \langle NJTT_z || r_{p/n}^2 Y_{20}(\hat{r}_{p/n}) || NJTT_z \rangle \quad (9a)$$

or

$$A(E2)_{p/n} = \sum_{\rho\rho'} D^{NJTT_z}(2,\rho,\rho') \times \langle \rho || r_{p/n}^2 Y_{20}(\hat{r}_{p/n}) || \rho' \rangle_{(t_z = t_z' = p/n)} . \quad (9b)$$

C. Formulation of single-particle matrix elements

It can be shown that the reduced single-particle matrix elements for $r^L Y_{LM}(\hat{r})$ can be factored as[10]

$$\langle \rho || r^L Y_{LM}(\hat{r}) || \rho' \rangle = \langle \rho \mid r^L \mid \rho' \rangle f^{(EL)}(lj;l'j') , \quad (10)$$

where $\langle \rho \mid r^L \mid \rho' \rangle$ is the radial integral and

$$f^{(EL)}(lj;l'j') = \tfrac{1}{2}(-1)^{j'+1/2} \langle j \, -\tfrac{1}{2} \, j' \, \tfrac{1}{2} \mid L\,0 \rangle \times [1+(-1)^{l+l'+L}] \times \sqrt{(2j+1)(2j'+1)/4\pi} . \quad (11)$$

Note that $f^{(EL)}(lj;l'j') = (-1)^{j-j'} f^{(EL)}(l'j';lj)$ and that for quadrupole moment calculations in the *sd* shell one

TABLE I. One-body-transition densities $D^{NJTT_z}(2,\rho,\rho')$ for the ground states and 2_1^+ states of various *sd*-shell nuclei as calculated from the wave functions of Ref. 6. Note that in the *sd* shell, one has $D^{NJTT_z}(2,\rho,\rho')=(-1)^{\rho+\rho'+1}D^{NJTT_z}(2,\rho',\rho)$.

		$(\rho\text{-}\rho')$					
$^AX(J_i^\pi)$	n/p	$(\frac{5}{2}\text{-}\frac{5}{2})$	$(\frac{5}{2}\text{-}\frac{1}{2})$	$(\frac{5}{2}\text{-}\frac{3}{2})$	$(\frac{1}{2}\text{-}\frac{3}{2})$	$(\frac{3}{2}\text{-}\frac{3}{2})$	$A(E2)$[a]
$^{17}O(\frac{5}{2}^+)$	n	1.0	0.0	0.0	0.0	0.0	−7.820
	p	0.0	0.0	0.0	0.0	0.0	0.0
$^{18}O(2_1^+)$	n	−0.0858	0.5222	0.0788	0.0613	0.0359	−7.833
	p	0.0	0.0	0.0	0.0	0.0	0.0
$^{18}F(5_1^+)$	n	1.0653	0.0	0.0	0.0	0.0	−8.447
	p	1.0653	0.0	0.0	0.0	0.0	−8.447
$^{18}F(\frac{5}{2}^+)$	n	0.5098	0.2560	0.1039	0.0830	0.0896	−9.877
	p	0.4757	0.1023	−0.0137	0.0543	0.0148	−5.793
$^{20}F(2_1^+)$	n	−0.2894	−0.1937	−0.1539	−0.0570	−0.0490	7.216
	p	−0.0650	−0.1117	−0.0673	−0.0470	−0.0300	3.326
$^{20}Ne(2_1^+)$	n	0.2998	0.3622	0.0975	0.1515	0.0855	−10.45
	p	0.2998	0.3622	0.0975	0.1515	0.0855	−10.45
$^{21}Ne(\frac{3}{2}^+)$	n	−0.2317	−0.3497	−0.1340	−0.0779	−0.0455	9.052
	p	−0.2314	−0.2690	−0.0448	−0.1101	−0.0435	7.545
$^{22}Ne(2_1^+)$	n	0.4748	0.3545	0.2397	0.1260	0.0230	−12.54
	p	0.2887	0.3591	0.0783	0.1000	0.0541	−9.610
$^{23}Na(\frac{3}{2}^+)$	n	−0.3330	−0.2438	−0.1811	−0.1049	−0.0083	9.079
	p	−0.2164	−0.3427	−0.1080	−0.0587	−0.0232	8.447
$^{24}Mg(2_1^+)$	n	0.4584	0.3460	0.2376	0.1356	0.0319	−12.71
	p	0.4584	0.3460	0.2376	0.1356	0.0319	−12.71
$^{25}Mg(\frac{5}{2}^+)$	n	−0.3482	−0.3210	−0.3077	−0.1338	−0.0793	12.42
	p	−0.6790	−0.3336	−0.2985	−0.1317	−0.0755	15.33
$^{26}Mg(2_1^+)$	n	−0.1004	0.1102	0.1152	0.1063	0.0326	−3.239
	p	0.4036	0.3339	0.1393	0.1321	0.0182	−11.33
$^{27}Al(\frac{5}{2}^+)$	n	−0.0465	−0.2713	−0.2172	−0.0633	−0.0916	7.721
	p	−0.6533	−0.1917	−0.2337	−0.1463	−0.0996	13.07
$^{28}Si(2_1^+)$	n	−0.3631	−0.3875	−0.2880	−0.0869	−0.1569	13.70
	p	−0.3631	−0.3875	−0.2880	−0.0869	−0.1569	13.70
$^{30}Si(2_1^+)$	n	0.0102	−0.0681	−0.1241	0.1248	0.4901	−2.864
	p	−0.1645	−0.0925	−0.0060	−0.0156	−0.0742	3.654
$^{32}S(2_1^+)$	n	0.0263	0.0827	0.0288	0.2915	0.4143	−8.381
	p	0.0263	0.0827	0.0288	0.2915	0.4143	−8.381
$^{33}S(\frac{3}{2}^+)$	n	0.0591	0.0643	0.0822	0.1152	0.6042	−8.052
	p	0.0749	0.0703	0.1161	0.1309	−0.0292	−4.330
$^{34}S(2_1^+)$	n	−0.0613	−0.0899	0.0100	−0.4029	−0.2126	8.592
	p	−0.0411	−0.1234	−0.1281	−0.0517	0.3225	1.891
$^{35}S(\frac{3}{2}^+)$	n	−0.0020	−0.0089	−0.0046	−0.0069	−0.9021	6.767
	p	−0.0437	−0.0196	−0.0800	−0.1042	0.0138	2.726
$^{35}Cl(\frac{3}{2}^+)$	n	0.0620	0.0557	0.0698	0.1398	0.4720	−7.322
	p	0.0568	0.0598	0.0985	0.1281	0.4039	−6.967
$^{36}S(2_1^+)$	n	0.0	0.0	0.0	0.0	0.0	0.0
	p	0.0009	0.0595	−0.0244	0.2272	0.8695	−9.982
$^{36}Cl(2_1^+)$	n	0.0014	−0.0006	−0.0430	0.0149	−0.0022	0.224
	p	−0.0037	0.0084	−0.0325	0.0006	−0.0109	0.280
$^{36}Ar(2_1^+)$	n	−0.0612	−0.1281	−0.0221	−0.3717	−0.2855	9.757
	p	−0.0612	−0.1281	−0.0221	−0.3717	−0.2855	9.757
$^{37}Cl(\frac{3}{2}^+)$	n	0.0	0.0	0.0	0.0	0.0	0.0
	p	0.0234	0.0065	0.0441	0.0791	0.9121	−8.431
$^{38}Ar(2_1^+)$	n	0.0	0.0	0.0	0.0	0.0	0.0
	p	−0.0010	−0.0177	0.0631	−0.2823	−0.0403	3.728
$^{39}K(\frac{3}{2}^+)$	n	0.0	0.0	0.0	0.0	0.0	0.0
	p	0.0	0.0	0.0	0.0	−1.0	7.385

[a]The values of the matrix elements $A(E2)$ defined in Eq. (8d) (units of fm^2) are calculated using the harmonic oscillator potential with $\hbar\omega=45A^{-1/3}-25A^{-2/3}$ (MeV).

has l and l' equal to 0 or 2 (and therefore even), and $L=2$. Hence $f^{(E2)}(j;j')$, with l and l' suppressed, reduces to

$$f^{(E2)}(j;j')=(-1)^{j'+1/2}\langle j-\tfrac{1}{2}j'\tfrac{1}{2}\,|\,20\rangle \times\sqrt{2j+1)(2j'+1)/4\pi}\,. \tag{12}$$

The values of $f^{(E2)}(j;j')$ for the *sd* shell are given in Table II. The radial wave functions in Eq. (10) typically are calculated from a central potential. If we assume a spherical harmonic oscillator potential, $V(r)=\frac{1}{2}m\omega^2r^2$ (where m is the proton mass), then the single-particle radial wave functions $R_{nl}(r)$ are given in terms of the length parameter b ($b^2=\hbar/m\omega$) by standard formulae [see, for example, Eqs. (2.21) and (2.23) in Ref. 10]. In the *sd* shell we have $|\,d\rangle=R_{12}(r)$ and $|\,s\rangle=R_{20}(r)$, which leads to the following expressions for the single-particle radial matrix elements:

$$\langle d\,|\,r^L\,|\,d\rangle=\frac{8b^L}{15\sqrt{\pi}}\Gamma[(L+7)/2]\,, \tag{13a}$$

$$\langle d\,|\,r^L\,|\,s\rangle=\frac{-2(L+2)\sqrt{2}b^L}{3\sqrt{5\pi}}\Gamma[(L+5)/2]\,, \tag{13b}$$

where $\Gamma(x)$ is the gamma function. Equations (13a) and (13b) (for $L=2$) reduce to $\langle d\,|\,r^2\,|\,d\rangle=3.5b^2$ and $\langle d\,|\,r^2\,|\,s\rangle=-\sqrt{10}b^2$.

The value of b can be obtained from the rms point proton radius r_p for nuclei in the *sd* shell via the expression[11]

$$r_p^2=\left[\frac{18+3.5(Z-8)}{Z}\right]b^2-\frac{3b^2}{2A}\,, \tag{14}$$

where the rms charge radius r_{ch} is related to r_p^2 via the equation[12]

$$r_{ch}^2=r_p^2+r_{proton}^2+(N/Z)r_{neutron}^2+\tfrac{3}{4}(\hbar/mc)^2\,. \tag{15}$$

In this work we take $r_{proton}^2=(0.86)^2$ and $r_{neutron}^2=-(0.34)^2$.

The experimental rms charge radii for stable *sd*-shell nuclei and their corresponding b values are given in Ref. 3. They are also presented here in the No. 2 entries of Table III. These experimental r_{ch} values are plotted versus mass number A in Fig. 1. An estimate for the dependence of the oscillator parameter upon mass number which yields a reasonably accurate fit to data for closed-shell nuclei is given[11] by

$$\hbar\omega=45A^{-1/3}-25A^{-2/3}\ (\text{MeV})\,, \tag{16}$$

or, equivalently,

$$b=0.960A^{1/6}[1-(0.556)A^{-1/3}]^{-1/2}\ (\text{fm})\,. \tag{17}$$

The b values from this expression, when put into Eqs. (14) and (15), produce rms charge radii which are also plotted in Fig. 1. It can be seen that while this formula reproduces the overall trends of the experimental values of r_{ch}, some data, particularly around ^{20}Ne, deviate appreciably from the smooth trend.

The conventional alternatives to harmonic oscillator single-particle wave functions are obtained from Saxon-Woods potentials. The Saxon-Woods potential must be specified in terms of several parameters, the choices of which can affect the relative as well as absolute values of the rms radii of the individual single-particle wave functions. In this study we utilize a local Saxon-Woods potential which is parametrized according to the approach of Ref. 13. The spin-orbit radii and diffusivities are set equal to the corresponding central values, and values of the well depth, radius, and diffusivity of the central potential are fixed independently for ^{16}O and ^{40}Ca so as to give agreement with the data on the charge distribution and single-particle separation energies for these systems. Parameters for nuclei in the interior of the *sd* shell are then determined by a smooth interpolation ($X=\alpha+\beta A^{1/3}$) between the ^{16}O and ^{40}Ca values. This choice of parametrization for the Saxon-Woods potentials gives an accounting of experimental r_{ch} values (also shown in Fig. 1) which is analogous to that provided by the oscillator parametrization of Eq. (16), although the oscillator parametrization is not so focused on reproducing precisely the ^{16}O and ^{40}Ca radii.

The different potential formulations yield different relative values of the rms radii for the individual $nljt_z$ orbits. For nuclei with only a few *sd*-shell particles, the values of r_{ch} are dominated by the protons in the $0s$ and $0p$ shells. Hence, the rms radii of the *sd* orbits from the two prescriptions of the potential can be appreciably different and not affect the value of r_{ch} significantly. As we progress to nuclei with more *sd*-shell nucleons, however, the values of r_{ch} depend more and more on the rms radii of the *sd* orbits themselves. Hence, the requirement that the theoretical value of r_{ch} in each model fits the ^{40}Ca radius has the consequence that the oscillator and Saxon-Woods values of the rms radii of the *sd* orbits are essentially equal to each other at $A=40$.

A finite-depth potential such as the Saxon-Woods can in principle be parametrized to take account of specific binding-energy effects. These effects should be especially important for proton-rich states for which the separation energy is small. The smooth variation with mass that is used here does not account for these individual variations, so this particular rationale for choosing a Saxon-Woods over an oscillator potential is not exploited. The present Saxon-Woods formulation, however, is systematically dif-

TABLE II. Values of the expression $f^{(E2)}(\rho,\rho')$ and $\langle\rho\,|\,r^2\,|\,\rho'\rangle$ as defined in Eqs. (12) and (13), respectively, for the single-particle orbits of the *sd* shell.

$(\rho\text{-}\rho')$	$(\frac{5}{2}\text{-}\frac{5}{2})$	$(\frac{5}{2}\text{-}\frac{1}{2})$	$(\frac{5}{2}\text{-}\frac{3}{2})$	$(\frac{1}{2}\text{-}\frac{3}{2})$	$(\frac{3}{2}\text{-}\frac{3}{2})$
$f^{(E2)}(\rho,\rho')$	−0.7378	0.6910	−0.3693	0.5642	−0.5642
$\langle\rho\,\|\,r^2\,\|\,\rho'\rangle$	$3.5b^2$	$-\sqrt{10}b^2$	$3.5b^2$	$-\sqrt{10}b^2$	$3.5b^2$

TABLE III. Calculated and experimental electric quadrupole moments in units of e fm^2. Calculation No. 1 uses the harmonic oscillator potential with $\hbar\omega = 45A^{-1/3} - 25A^{-2/3}$ (MeV) and No. 2 uses the harmonic oscillator (HO) potential with b values obtained from r_{ch} (experiment) for each stable nucleus. In these two calculations, the effective charges are $\tilde{e}_p = 1.35e$ and $\tilde{e}_n = 0.35e$. Calculation No. 3 uses a Saxon-Woods (SW) potential with effective charges of $\tilde{e}_p = 1.15e$ and $\tilde{e}_n = 0.45e$.

$^AX(J^\pi)$	Calc.	Potential	r_{ch} (fm)	b (fm)	Q (theor.)	Q (expt.)[a]
$^{17}O(\frac{5}{2}^+)$	1	HO	2.676	1.739	−2.12	−2.58±0.05
	2	HO	2.712	1.765	−2.18	
	3	SW	2.684		−3.13	
$^{17}F(\frac{5}{2}^+)$	1	HO	2.766	1.739	−8.17	±10±2
	2	HO	2.801	1.763	−8.39	
	3	SW	2.889		−8.70	
$^{18}O(2_1^+)$	1	HO	2.689	1.751	−2.08	−2±3[b]
	2	HO	2.794	1.826	−2.26	
	3	SW	2.664		−3.59	
$^{18}F(5_1^+)$	1	HO	2.781	1.751	−10.43	±13±2
	2	HO	2.882	1.821	−11.27	
	3	SW	2.842		−11.00	
$^{19}F(\frac{5}{2}^+)$	1	HO	2.794	1.763	−8.72	−12±2
	2	HO	2.897	1.833	−9.43	
	3	SW	2.813		−9.85	
$^{20}F(2_1^+)$	1	HO	2.807	1.774	5.32	7.0±1.3
	2	HO	2.946	1.869	5.90	
	3	SW	2.792		6.22	
$^{20}Ne(2_1^+)$	1	HO	2.880	1.774	−13.46	−23±3[b]
	2	HO	3.020	1.867	−14.92	
	3	SW	2.942		−14.81	
$^{21}Ne(\frac{3}{2}^+)$	1	HO	2.893	1.785	9.47	10.3±0.8
	2	HO	2.984	1.845	10.12	
	3	SW	2.917		10.29	
$^{22}Ne(2_1^+)$	1	HO	2.906	1.795	−13.16	−19±4
	2	HO	2.949	1.824	−13.58	
	3	SW	2.899		−13.86	
$^{23}Na(\frac{3}{2}^+)$	1	HO	2.979	1.805	10.34	10.06±0.20[c]
	2	HO	2.986	1.810	10.39	
	3	SW	3.004		10.65	
$^{24}Mg(2_1^+)$	1	HO	3.041	1.815	−16.38	−18±2[b]
	2	HO	3.035	1.811	−16.31	
	3	SW	3.098		−16.82	
$^{25}Mg(\frac{5}{2}^+)$	1	HO	3.053	1.824	19.37	20.1±0.3[d]
	2	HO	3.003	1.792	18.69	
	3	SW	3.078		18.97	
$^{26}Mg(2_1^+)$	1	HO	3.065	1.834	−12.45	−13±3[e]
	2	HO	3.017	1.803	−12.04	
	3	SW	3.062		−11.34	
$^{27}Al(\frac{5}{2}^+)$	1	HO	3.119	1.843	15.74	15.0±0.6[d]
	2	HO	3.058	1.804	15.08	
	3	SW	3.142		14.86	
$^{28}Si(2_1^+)$	1	HO	3.168	1.851	17.65	16±3[b]
	2	HO	3.125	1.824	17.14	
	3	SW	3.215		17.35	
$^{30}Si(2_1^+)$	1	HO	3.199	1.868	2.98	−5±6[b]
	2	HO	3.137	1.829	2.86	
	3	SW	3.190		2.17	
$^{32}S(2_1^+)$	1	HO	3.271	1.884	−10.80	−16±2[f]
	2	HO	3.263	1.879	−10.74	
	3	SW	3.335		−10.42	
$^{33}S(\frac{3}{2}^+)$	1	HO	3.285	1.891	−6.14	−6.4±1.0
	2	HO	3.264	1.878	−6.06	
	3	SW	3.321		−6.10	

TABLE III. (*Continued*).

$^AX(J^\pi)$	Calc.	Potential	r_{ch} (fm)	b (fm)	Q (theor.)	Q (expt.)[a]
$^{34}S(2_1^+)$	1	HO	3.300	1.899	4.21	4±3[b]
	2	HO	3.264	1.877	4.12	
	3	SW	3.311		4.55	
$^{35}S(\frac{3}{2}^+)$	1	HO	3.311	1.906	4.29	4.5±1.0
	2	HO	3.335	1.921	4.36	
	3	SW	3.303		4.32	
$^{35}Cl(\frac{3}{2}^+)$	1	HO	3.331	1.906	−8.49	−8.249±0.002
	2	HO	3.351	1.919	−8.60	
	3	SW	3.360		−7.96	
$^{36}S(2_1^+)$	1	HO	3.322	1.913	−10.21	
	2	HO	3.363	1.938	−10.48	
	3	SW	3.297		−8.27	
$^{36}Cl(2_1^+)$	1	HO	3.342	1.913	0.346	−1.80±0.04
	2	HO	3.382	1.938	0.355	
	3	SW	3.350		0.317	
$^{36}Ar(2_1^+)$	1	HO	3.359	1.913	12.57	11±6[b]
	2	HO	3.399	1.937	12.89	
	3	SW	3.407		11.81	
$^{37}Cl(\frac{3}{2}^+)$	1	HO	3.353	1.920	−8.07	−6.493±0.002
	2	HO	3.351	1.919	−8.06	
	3	SW	3.344		−6.64	
$^{38}Ar(2_1^+)$	1	HO	3.381	1.927	3.81	
	2	HO	3.414	1.947	3.89	
	3	SW	3.388		3.14	
$^{39}K(\frac{3}{2}^+)$	1	HO	3.410	1.934	7.07	5.2±0.3
	2	HO	3.437	1.950	7.19	
	3	SW	3.431		5.96	

[a]All entries not otherwise referenced are taken from the compilation of Ref. 18.
[b]Taken from the compilations of Ref. 29.
[c]Reference 22.
[d]Reference 23.
[e]Average from Refs. 29 and 32.
[f]Average from Refs. 34–36, assuming constructive interference. Note that the uncertainty in the weighted value is significantly smaller than each individual measured uncertainty.

ferent from the analogous oscillator results in that the proton radii for any given system are larger than the associated neutron radii because of the repulsive Coulomb potential. The consequences of this for the full $E2$ operator will be discussed in the next section.

D. Effective charges

Calculation of a nuclear observable such as the electric quadrupole moment in terms of the matrix elements of an operator evaluated between a limited range of single-particle states of the shell model, as defined in Eq. (5), implies a correspondence between this "model" matrix element and the "true" matrix element, for which the sum over single-particle states is unlimited. It is desired, obviously, that the "true" and the "model" matrix elements be equal. Since it is unlikely that the contributions from orbits excluded from the model space are exactly zero, the "model" operator must hence differ from the "true," or "free-space" operator to compensate for the model-space truncations.

The configurations excluded by the *sd*-shell model which presumably are most important for a complete description of $E2$ phenomena are those which incorporate one-particle, one-hole excitations from the $0s$ to the $0d,1s$ orbits, from the $0p$ to the $0f,1p$ orbits, and from the $0d,1s$ to the $0g,1d,2s$ orbits. These particle-hole excitations, acting coherently, are the basis of the so-called "giant $E2$ resonance," which is found in all nuclei at an energy of approximately $E=65A^{-1/3}$ MeV and which has a strength comparable to that of the strong $E2$ excitations between low-lying nuclear levels. These same one-particle, one-hole excitations should also affect the strength of the $E2$ matrix elements between low-lying states, even though the admixtures of such configurations into the wave functions are quite small.

This general problem manifests itself in the case of the *sd*-shell and electric quadrupole moments in the classic example of ^{17}O. The conventional shell-model truncation for *sd*-shell nuclei corresponds to the assumptions that ^{16}O forms an inert core for $8\leq N,Z\leq 20$ nuclei and that the single-particle orbits lying higher in energy than the *sd* orbits are completely vacant. With this model and with the free-space ($e_p=1e$ and $e_n=0e$) $E2$ operator, the

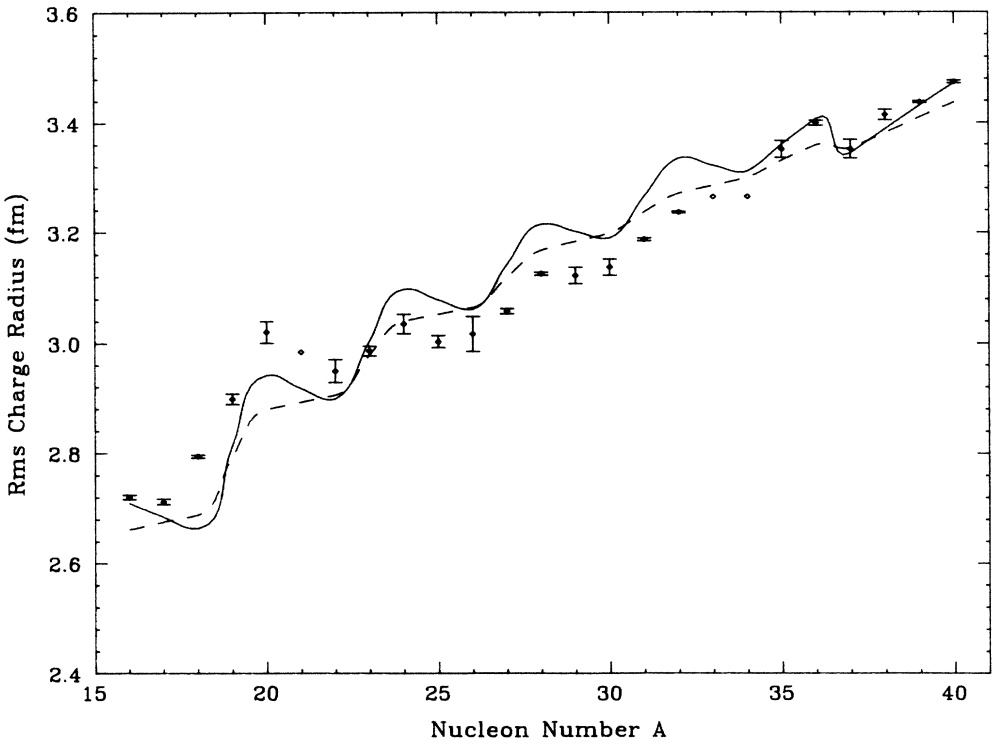

FIG. 1. Comparison of experimental values of r_{ch} with predictions from Saxon-Woods (solid line) and harmonic oscillator (dashed line) ($\hbar\omega = 45A^{-1/3} - 25A^{-2/3}$ MeV) potentials.

quadrupole moment of the ground state of ^{17}O must be zero, since the ground state of ^{17}O is modeled purely in terms of a single neutron. (It likewise follows that *sd*-shell model wave functions for all states of the oxygen isotopes have vanishing quadrupole moments.) However, the quadrupole moment of the ground state of ^{17}O is found experimentally to be not zero but -2.58 ± 0.05 e fm^2. Hence, the $E2$ operator must be renormalized if the *sd* orbits of the shell model are to be able to deal quantitatively with these experimental data. Further study shows that observed $E2$ matrix elements in all nuclei tend to be larger than the predictions of shell-model wave functions when the protons and neutrons of the model are given charges of $1e$ and $0e$, respectively.

The simplest procedure by which shell-model matrix elements for electric quadrupole observables can be brought into agreement with experiment is to assign "effective" charges, $\tilde{e}_p$ and $\tilde{e}_n$, to the protons and neutrons which are active in the model space. The ^{17}O problem, for example, is thus solved tautologically by having the $d_{5/2}$ neutron carry a charge of the appropriate magnitude. The test of the efficacy of this simple approach is whether a sequence of states with different N and Z values is consistent with values of $\tilde{e}_p$ and $\tilde{e}_n$ which are constant or slowly varying.

As a procedure for renormalizing shell-model $E2$ matrix elements for the effect of excluded configurations, this effective charge model is extremely simple. It could be expected that each single-particle orbit or single-particle matrix element might require its own individual renormalization and that these renormalizations might depend strongly on the individual masses and states.[14–16] State dependence is particularly strong for $A=17$ where the effective charge is smaller for states that are loosely bound.[14,15] However, for well-bound states, the state dependence as obtained in recent random-phase approximation (RPA) Hartree-Fock calculations is weak.[15] The effective charge is also expected to increase as a function of mass in going from the beginning to the end of the *sd* shell,[14–16] and there is some experimental evidence for this increase.[16]

However, on the whole, the *sd* shell experimental data on $E2$ transitions are consistent with an effective charge which is constant, independent of state and mass.[13,16] Thus, as a working hypothesis we will present comparisons of the experimental quadrupole moment data with theoretical matrix elements in which the free-space charges of the proton and neutron ($1e$ and $0e$) are replaced by the constant effective charges $\tilde{e}_p = e + \Delta e_p$ and $\tilde{e}_n = \Delta e_n$, respectively. Any deviation between experiment and theory might then be ascribed to a breakdown of this assumption about the effective charge and/or to a deficiency in the multiparticle wave functions.

As is obvious from Eqs. (8d) and (9b), the model values of electric quadrupole moments depend on the assumptions about the radii of the single-particle wave functions and about the charges on the model particles in a correlated fashion. In our empirical approach the effective charges are the parameters by which the model $E2$ matrix elements $A(E2)_p$ and $A(E2)_n$ are normalized to optimize their agreement with experimental data. Different choices for single-particle wave functions presuppose different

values for the effective charges. In this study we follow the conclusions of Ref. 13 for the optimum values of effective charges for the *sd*-shell space and the parametrizations of single-particle radial wave functions described above.

For the harmonic-oscillator radial prescriptions the optimum values from Ref. 13 are $\Delta e_p = \Delta e_n = 0.35e$. These effective charges are used here for calculations which use oscillator wave functions with b values given by Eq. (17) (results labeled No. 1 in Table III) and, alternatively, b values chosen to fit the individual experimental values of r_{ch} for each A value (results labeled No. 2 in Table III). The consequences of using this same choice for effective charges with the Saxon-Woods radial wave functions are $E2$ matrix elements which are larger than the corresponding oscillator values at the beginning of the shell and very nearly equal to most of the oscillator values above $A = 30$.

The conclusions of Refs. 13 and 14 are that, when using Saxon-Woods wave functions, the value of Δe_p should be smaller than the value of Δe_n for *sd*-shell nuclei. The actual choices from Ref. 13 are $\Delta e_p = 0.15$ and $\Delta e_n = 0.45e$. These values reflect rms radii for the Saxon-Woods *sd*-shell orbits which are larger on the average than the corresponding oscillator radii and proton radii which are larger than neutron radii. The consequences for $E2$ matrix elements of using these values of effective charge (results labeled No. 3 in Table III) differ from the results No. 1 and No. 2 principally for states which are pure proton or pure neutron configurations in the model context.

E. Summary and discussion of the theory

The procedure for calculating model values of $Q(J^\pi, {}^A X)$ is clear from the preceding discussion. Values of the single-particle matrix elements $\langle \rho || r^2 Y_{20}(\hat{r}) || \rho' \rangle$ are obtained according to Eq. (10) by using the values of $f^{(E2)}(j;j')$ from Eq. (12) (values given in Table II) and by adopting a model for the radial wave functions which ensures that the observed nuclear radii are approximately reproduced. These single-particle matrix elements are then combined according to Eq. (9b) with the one-body-transition densities defined in Eq. (6) (values for each $AJTT_z$ given in Table I) in order to obtain the full proton and neutron matrix elements $A(E2)_{p/n}$. These multiparticle matrix elements then are combined with $\tilde{e}_p$ and $\tilde{e}_n$ according to Eq. (8d) to obtain the quadrupole moments Q. It is important to emphasize that the sum in Eqs. (5) and (9b) must be over *all* (j,j') pairs in the model space; i.e., both the (j,j') and (j',j) combinations for an orbit pair with j different from j' must be included.

In the present calculations, the basis vectors Φ are represented as

$$\Phi(NJT) = \{ [(d_{5/2})^{n_1 J_1 T_1} \times (s_{1/2})^{n_2 J_2 T_2}]^{J_{12} T_{12}} \times (d_{3/2})^{n_3 J_3 T_3} \}^{NJT},$$

where $n_1 + n_2 + n_3 = N = A - 16$ and the $n_i J_i T_i$ give the number of nucleons in the orbit j_i and the values of the internal angular momentum and isospin couplings in that orbit. An eigenfunction Ψ of the model is then

$$\Psi(NJT) = \sum_i^d a_i \Phi_i(NJT),$$

where the sum runs over the basis states $\Phi_i(NJT)$ up to the dimension d. In the present calculations, the model spaces uniformly include every basis state that can be constructed from the three *sd*-shell orbits.

The features of $E2$ matrix elements predicted in this model can be traced back to the number and identity of the single-particle orbits ρ which define the model space, and to the distribution of probability over the various basis vectors. The orbits of the *sd*-shell yield 16 one-body density, $D^{NJTT_z}(2,\rho,\rho')$, combinations for the $E2$ operator. The $s_{1/2}s_{1/2}$ combination is forbidden because of angular-momentum constraints. The inequivalent-orbit combinations ρ-ρ' and ρ'-ρ have equal magnitudes in the situations treated here, since the initial-state and final-state wave functions are identical. The relative signs of the $D^{NJTT_z}(2,\rho,\rho')$ and $D^{NJTT_z}(2,\rho',\rho)$ pairs coincide with those of their associated single-particle matrix elements, so that each pair need be specified only by a single value. In the ρ-ρ' sequences listed in Tables I and II, the single-particle matrix values all have the same sign. Hence, it is obvious from the signs listed in Table I whether the various one-body contributions to the value of a total moment combine constructively or destructively. The magnitudes of the single-particle matrix elements of the *sd*-shell orbits differ from each other by at most a factor of 2. Hence, a one-body-density contribution from any given pair of orbits is approximately equivalent to that from any other pair in constructing the total matrix element.

The essence of configuration-mixing shell-model calculations is the detailed distribution of probability over the individual basis vectors $\Phi_i(NJT)$. It is instructive to consider the mixed-configuration wave function which results from diagonalizing the model Hamiltonian in comparison to the "*jj*-limit" wave function corresponding to the single $\Phi_i(NJT)$ which corresponds to filling the model orbits in the conventional *jj*-coupling sequence. As a simple example, the *jj*-limit wave function for the first 2^+ state of ^{18}O would be $(d_{5/2})^{2,J=2}$. The configuration-mixed wave function for this state has a probability of 61% for the $(d_{5/2})^2$ component and a 32% probability for the $(d_{5/2})^1$-$(s_{1/2})^1$ component, the remaining probability being distributed over the $(d_{5/2})^1$-$(d_{3/2})^1$, $(s_{1/2})^1$-$(d_{3/2})^1$, and $(d_{3/2})^2$ components.

For quadrupole moment calculations in *jj*-coupling representation, the vital difference between the "configuration-mixed" wave function $\Psi(NJT)$ and any single-component wave function $\Phi_i(NJT)$ is that the former allows one-body-density terms for which $\rho \neq \rho'$, while the latter does not. This difference is not a function of the constitution of the particular single component, but results just because it is impossible to annihilate a particle ρ from a basis vector $\Phi_i(NJT)$, create a different kind of particle ρ', and then return to the same $\Phi_i(NJT)$. By the same token, the one-body-density terms with $\rho \neq \rho'$ can originate *only* by connecting one basis vector $\Phi_i(NJT)$ to a different one. Also, obviously, basis vectors which differ in orbit occupations by more than one particle or hole cannot be connected by any one-body operator pair.

The consequences of this difference between single-component *jj*-limit and many-component configuration-mixed wave functions for the value of Q are profound. For example, the value of the quadrupole moment from the *jj*-limit wave function for ^{18}O is $+1.23\ e\,\mathrm{fm}^2$, while for the actual configuration-mixed wave function the value is $-2.08\ e\,\mathrm{fm}^2$. The values of $D^{NJTT_z}(2,\rho,\rho')$ for the *jj*-limit wave function are -0.583 for $\rho\text{-}\rho'=\frac{5}{2}\text{-}\frac{5}{2}$ and zero for all others. For the mixed configuration wave functions (see Table I), the dominant term is $D^{NJTT_z}(2,\frac{5}{2},\frac{1}{2})$, with a value of $+0.522$; the value of $D^{NJTT_z}(2,\frac{5}{2},\frac{5}{2})$, along with the others, is an order of magnitude smaller. Thus, a 32% admixture of the secondary configuration into the wave function results in a reversal of the sign of the moment from positive to negative. The origins of this reversal are twofold. First, the 32% $(d_{5/2})^1\text{-}(s_{1/2})^1$ component yields a $D^{NJTT_z}(2,\frac{5}{2},\frac{5}{2})$ contribution that largely cancels the contribution from the 61% $(d_{5/2})^2$ component. Second, the $(d_{5/2})^2$ and the $(d_{5/2})^1\text{-}(s_{1/2})^1\text{-}(s_{1/2})^1$ components are connected (twice) by the $\rho\text{-}\rho'=\frac{5}{2}\text{-}\frac{1}{2}$ one-body operators to give a large $D^{NJTT_z}(2,\frac{5}{2},\frac{1}{2})$ contribution which has the opposite sign from that of the $D^{NJTT_z}(2,\frac{5}{2},\frac{5}{2})$ from $(d_{5/2})^2$.

The influence of configuration mixing upon predicted quadrupole moments is even more striking than in this ^{18}O illustration for cases in which the *jj*-limit wave function yields $L=2$ one-body densities which are identically zero because of a general selection rule. For example, in the "hole" analog of ^{18}O, ^{38}Ar, the basis vector of the first 2^+ state which has the largest amplitude (93%) is $(d_{3/2})^{-2}$. Due to the selection rule[17] that *E2 matrix elements between states of the same seniority vanish for a half-filled shell,* the value of $D^{NJTT_z}(2,\frac{3}{2},\frac{3}{2})$ for $(d_{3/2})^2$ is zero. This, not cancellation as in the case of ^{18}O, explains the small value of the $D^{NJTT_z}(2,\frac{3}{2},\frac{3}{2})$ for ^{38}Ar in Table I. (The deviation from zero comes from the contributions of the small components in the mixed-configuration wave function.) Given the dominance of the $(d_{3/2})^{-2}$ component in the wave function, the values of $D^{NJTT_z}(2,\rho,\rho')$, and hence the value of Q, depend very sensitively upon the magnitudes and relative signs of the $(d_{5/2})^{-1}\text{-}(d_{3/2})^{-1}$ and $(s_{1/2})^{-1}\text{-}(d_{3/2})^{-1}$ wave function components which connect with $(d_{3/2})^{-2}$.

The fact that $(d_{3/2})^2$ has an $L=2$ one-body density which is equal to zero is important for the entire range of states from ^{30}Si on up to ^{38}Ar, because it is an important, often dominant, component of the wave functions for all of these nuclei. Since their contributions to diagonal $D^{NJTT_z}(2,\rho,\rho)$ values vanish, these wave function components contribute to the values of the quadrupole moments only through off-diagonal $D^{NJTT_z}(2,\rho,\rho')$ terms, in proportion to the amplitudes of typically much smaller components. The consequence is an extreme sensitivity of the predicted values of Q to the details of configuration mixing in the individual wave functions.

Beyond the specific dramatic effects just described, configuration mixing also typically creates an enhancement in the predicted magnitude of Q over the value which can be obtained with any corresponding *jj*-limit, single-component, wave function. Of course, this coherent amplification is under the control of the model Hamiltonian and the relative phases of the various components which it creates, but in the typical case for which the phases are "constructive," the amplification can be a factor of 3 to 4.

III. EXPERIMENTAL VALUES OF *sd*-SHELL QUADRUPOLE MOMENTS

We concern ourselves in the present study with values of electric quadrupole moments which are determined with (nuclear) model-independent experimental techniques. The classic quadrupole moment experiments are based on measurements of the hyperfine splittings of atomic spectra. Values are summarized in standard compilations of nuclear data[18] and are listed here in Table III. These traditional "electronic" values of Q incorporate difficult to quantify and potentially serious systematic uncertainties which arise in converting observed line splittings into the inferred quadrupole-moment magnitudes. The difficulty lies in calculating the precise value at the nucleus of the electric field from the surrounding atomic electron configuration, as this configuration is perturbed by the nuclear moments themselves.[19,20] It is not easy to evaluate the quoted values of quadrupole moments derived from older atomic-spectra measurements because of the uncertainties in these "Sternheimer corrections." Without extensive reanalysis of these older measurements, the uncertainties to be associated with the quoted experimental values from this effect may be $1\ e\,\mathrm{fm}^2$ or larger. New measurements[21] with laser spectroscopy techniques have yielded quadrupole moment values for the ^{33}S, ^{35}Cl, and ^{37}Cl ground states which are consistent with the older values listed in Table III.

Muon-production facilities at high-intensity, medium-energy proton accelerators have made it possible to utilize muonic atoms in modern analogs of the traditional electronic-atom measurements. These "muonic" measurements provide values of quadrupole moments free from the dominant source of systematic uncertainty in the electronic values, since the relevant muon orbits are both significantly larger than the size of the nucleus and significantly smaller than the atomic K shell. The values of the electric gradients at the nucleus in the muonic atom are hence straightforward to calculate. Recent measurements[22,23] at SIN have provided values of the ground-state quadrupole moments of ^{23}Na, ^{25}Mg, and ^{27}Al. These values, also listed in Table III, are the experimental fulcrum of the present study. Perhaps more important than the values themselves, however, is the confidence in the estimation of their uncertainties. Additional measurements of other nuclei with the same technique would be extremely valuable.

Electric quadrupole moments of nuclear states which are unstable to β or γ emission can be studied in nuclear-magnetic-resonance experiments if the nuclei can be imbedded in a crystal structure which creates an appropriately strong, nonisotropic and known electric field. The magnitudes of the values for the fluorine isotopes have been obtained[24–26] in a series of such measurements and are also included in Table III.

There are two methods for measuring electric quadrupole moments of nuclear states which circumvent the need to know the electric field from the electronic, the analogous muonic, or the solid-state crystal structure which surrounds the nucleus. Elastic electron scattering experiments[27] can determine in principle all the multipole moments of the nuclear ground state. In practice, however, the uncertainties in the determination of the monopole charge distributions are such as to render the uncertainty in the associated quadrupole moment values uncompetitively large.

The "reorientation effect" technique,[28] which utilizes the Coulomb scattering of heavy ions, provides a method for determining the electric quadrupole moments of excited nuclear states. In reorientation-effect measurements, the observed small deviations from the pattern of the purely Coulomb inelastic scattering associated with the electric-quadrupole excitation from the 0^+ ground state to the 2^+ first-excited state are interpreted as the consequences of the higher-order coupling of this excitation to the quadrupole moment of the 2^+ state. The sign and magnitude of the deviation then yields the sign and magnitude of the moment. This method has been applied to determine the quadrupole moments of the $J^\pi=2^+$, first-excited states of almost all doubly-even nuclei of the *sd* shell.[29] These values are also presented in Table III.

It typically is difficult to achieve high statistical accuracy in reorientation-effect measurements, particularly when care is taken that the bombarding energies are low enough to ensure that the scattering process is purely Coulomb and thus not contaminated by nuclear effects. The technique is complicated in that the perturbation of the excitation of $0^+_{g.s.}$ to the 2^+_1 state by its coupling to $Q(2^+_1)$ is of the same order as the second-order excitations of 2^+_1 through higher-lying states. The dominant term of this type in the typical case is proportional to the product of the three $E2$ matrix elements,[28] $M(E2;0^+_{g.s.}\rightarrow 2^+_1)$, $M(E2;0^+_{g.s.}\rightarrow 2^+_2)$, and $M(E2;2^+_1\rightarrow 2^+_2)$, but higher 2^+ states and 4^+ states can also be important. These terms contribute uncertainties to the extracted value of $Q(2^+_1)$, since, while the magnitudes of these matrix elements might be experimentally determined, their signs are not.

The experimental values of $Q(2^+_1)$ obtained from reorientation-effect measurements are often quoted as a function of the assumed relative sign of the competing second-order corrections. If the product p_3 of the three matrix elements $M(E2;0^+_{g.s.}\rightarrow 2^+_1)M(E2;0^+_{g.s.}\rightarrow J^+_x)M(E2;2^+_1\rightarrow J^+_x)$ is negative ("destructive interference"), which decreases the scattering cross sections, a positive increment should be added to the value of the quadrupole moment extracted from the deviation of the observed cross sections from the pure Coulomb predications; likewise, if the product p_3 is positive (constructive interference), a negative increment should be added to the extracted value of Q.

The shell-model wave functions provide predictions of these matrix elements and their (relative) signs along with other observables. Such predictions for $J^\pi_x=2^+_2$ are presented in Table IV, along with the signs of the product p_3. It should be noted that the reliability of these predictions is questionable in many instances. For nuclei near

TABLE IV. Calculated $E2$ matrix elements connecting the 2^+_1 and 2^+_2 states in doubly-even *sd*-shell nuclei to each other and to the 0^+ ground state.

^AX	$J^\pi_i\rightarrow J^\pi_f$	$M(E2;J^\pi_i\rightarrow J^\pi_f)$[a] ($e$ fm^2)
^{18}O	$0^+_{g.s.}\rightarrow 2^+_1$	−3.43
	$0^+_{g.s.}\rightarrow 2^+_2$	−0.67
	$2^+_1\rightarrow 2^+_2$	−3.09
		p_3: −
^{20}Ne	$0^+_{g.s.}\rightarrow 2^+_1$	−16.41
	$0^+_{g.s.}\rightarrow 2^+_2$	0.38
	$2^+_1\rightarrow 2^+_2$	−4.43
		p_3: +
^{22}Ne	$0^+_{g.s.}\rightarrow 2^+_1$	−15.21
	$0^+_{g.s.}\rightarrow 2^+_2$	−4.47
	$2^+_1\rightarrow 2^+_2$	1.14
		p_3: +
^{24}Mg	$0^+_{g.s.}\rightarrow 2^+_1$	18.60
	$0^+_{g.s.}\rightarrow 2^+_2$	−5.56
	$2^+_1\rightarrow 2^+_2$	−8.69
		p_3: +
^{26}Mg	$0^+_{g.s.}\rightarrow 2^+_1$	17.35
	$0^+_{g.s.}\rightarrow 2^+_2$	3.00
	$2^+_1\rightarrow 2^+_2$	13.15
		p_3: +
^{28}Si	$0^+_{g.s.}\rightarrow 2^+_1$	8.46
	$0^+_{g.s.}\rightarrow 2^+_2$	1.09
	$2^+_1\rightarrow 2^+_2$	−6.84
		p_3: −
^{30}Si	$0^+_{g.s.}\rightarrow 2^+_1$	−13.97
	$0^+_{g.s.}\rightarrow 2^+_2$	−7.84
	$2^+_1\rightarrow 2^+_2$	17.97
		p_3: +
^{32}S	$0^+_{g.s.}\rightarrow 2^+_1$	14.91
	$0^+_{g.s.}\rightarrow 2^+_2$	−7.47
	$2^+_1\rightarrow 2^+_2$	−15.50
		p_3: +
^{34}S	$0^+_{g.s.}\rightarrow 2^+_1$	12.73
	$0^+_{g.s.}\rightarrow 2^+_2$	4.74
	$2^+_1\rightarrow 2^+_2$	−14.08
		p_3: −
^{36}S	$0^+_{g.s.}\rightarrow 2^+_1$	10.68
	$0^+_{g.s.}\rightarrow 2^+_2$	0.90
	$2^+_1\rightarrow 2^+_2$	−10.81
		p_3: −
^{36}Ar	$0^+_{g.s.}\rightarrow 2^+_1$	−15.64
	$0^+_{g.s.}\rightarrow 2^+_2$	1.09
	$2^+_1\rightarrow 2^+_2$	−9.84
		p_3: +
^{38}Ar	$0^+_{g.s.}\rightarrow 2^+_1$	12.00
	$0^+_{g.s.}\rightarrow 2^+_2$	6.06
	$2^+_1\rightarrow 2^+_2$	13.49
		p_3: −

[a]Values of $M(E2)$, defined as $M(E2)^2=(2J_i+1)B(E2)$, calculated with harmonic oscillator potential in prescription No. 2.

the shell boundaries, the model predictions for higher excited states do not correspond necessarily with the matching experimental states, since the experimental spectra have large "intruder state" contaminations. Moreover, in any instance of a small matrix element there is the possibility that the intrinsic uncertainty in the model results might also allow a comparably small matrix element of the opposite sign. Finally, in many cases there is no dominant second-order path to the 2_1^+ state, and the correction must come from a more complex sum over several such products. Nonetheless, the predicted signs of p_3 correspond to the choices made in analyzing all of the quadrupole moment data for which this correction is relevant.

Because of the variety of difficulties inherent both in acquiring and analyzing reorientation-effect data, the value chosen for a particular 2_1^+ state is often not a simple average over the different existing experimental values. In most cases the choices made for Table III parallel those of Spear in Ref. 29. We briefly discuss here our choices for these values.

The magnitude of the ^{18}O quadrupole moment is relatively small. As a consequence, the various corrections involved in reducing the data are important. This is reflected in the uncertainty of the value[29] quoted in Table III. The value quoted in Table III for ^{20}Ne is based on relatively old measurements, and the uncertainty perhaps does not reflect some sources of systematic error. The value[29] quoted for ^{22}Ne is based on experiments in which ^{20}Ne and ^{22}Ne were both measured. Hence, the ratio of the magnitudes of the two values, $Q(^{22}\text{Ne},2^+)/Q(^{20}\text{Ne},2^+) = 0.83$, should be more reliable than either individual value.

The value[29] quoted for ^{24}Mg is based on the two measurements for which nuclear interference with the Coulomb scattering is evaluated to be negligible. Some older, higher-energy, measurements give larger magnitudes. The value quoted in Table III for ^{26}Mg is the weighted average of the value quoted in Ref. 29 (the original data are from Refs. 30 and 31) and the value of Ref. 32. The value[29] quoted for ^{28}Si is based on relatively modern measurements and is consistent with the average of older measurements. The value listed for ^{30}Si is the result of a single measurement.[33] Its small magnitude makes it difficult to draw conclusions beyond the obvious one that the quadrupole moment of this state is small relative to the size of typical quadrupole moments and collective $E2$ matrix elements in this region.

The value of the quadrupole moment of the first 2^+ state of ^{32}S has been the subject of particular interest because of the possible vibrational nature of the low-lying energy levels of this system and because of the significant variations in the results of a sequence of different measurements. The value quoted in Table III is the weighted average of the results of Refs. 34–36. The value[29] quoted for ^{34}S is based on measurements done in conjunction with ^{32}S measurements. As such there should be good relative agreement between the values of the two nuclei. The key features of all the ^{34}S values are their small magnitudes and positive signs. The value of the quadrupole moment for the first 2^+ state of ^{36}Ar comes from a single measurement,[37] and there has been no measurement for the quadrupole moments of the first excited 2^+ states of ^{36}S and ^{38}Ar.

The quadrupole moments of the mass distribution of $J^\pi = 2^+$ excited states can be measured with intrinsically nuclear physics techniques[38] which are analogous to the reorientation-effect measurements of the charge-distribution quadrupole moments. Quoted values[38] for ^{24}Mg, ^{28}Si, and ^{32}S are $-14\ e\,\text{fm}^2$, $+17\ e\,\text{fm}^2$, and $-13\ e\,\text{fm}^2$, respectively, with uncertainties estimated at 20–40%. These values are consistent with those quoted in Table III. In addition, the signs of the interference products p_3 listed in Table IV are consistent with the assumptions of Ref. 38. Further development and exploitation of this technique may provide a valuable supplement to Coulomb reorientation-effect studies.

IV. COMPARISON OF THEORY WITH EXPERIMENT AND DISCUSSION OF RESULTS

Theoretical values of the electric quadrupole moments for *sd*-shell states, calculated as described in Sec. II, are presented and compared with experimental values in Table III. Results from combining the one-body-transition densities with three different combinations of single-particle radial wave functions and effective charges are given to illustrate the variations which can arise from this component of the calculation.

A. Trends of the predictions and relationships with previous results

1. *Ground states of stable odd-mass sd-shell nuclei*

As presented in Table III, the values of electric quadrupole moments for the ground states of the stable odd-mass nuclei of the *sd* shell (^{17}O, ^{21}Ne, ^{23}Na, ^{25}Mg, ^{27}Al, ^{33}S, ^{35}Cl, ^{37}Cl, and ^{39}K) calculated in the present study agree with the corresponding experimental values within the quoted (or estimated) uncertainties in almost every case. The calculations of Ref. 3 use the same full *sd*-shell space, the same effective-charge parametrization, and the same radial matrix element sizes as were employed in the present calculations to obtain the results labeled No. 2 in Table III. The differences between the present predictions and those of Ref. 3 thus must result from differences in configuration mixing induced by the different Hamiltonians used in the two studies, the Hamiltonian of Ref. 6 in the present case and the Chung-Wildenthal-particle (CWP) and Chung-Wildenthal-hole (CWH) Hamiltonians[39] in Ref. 3. Of course, the ^{17}O and ^{39}K results are independent of the Hamiltonian in the context of purely *sd* configurations and depend only on the radial matrix element and effective charge parametrizations, and so there are no differences at all in these instances.

The values of Q calculated in parametrization No. 2 for ^{21}Ne, ^{23}Na, and ^{35}Cl in the present work are very similar to the results of Ref. 3. The new calculated values of ^{25}Mg and ^{27}Al are slightly larger than the older results and, in each case, are in slightly better agreement with experiment. The new value for ^{33}S is smaller in magnitude than the older result, the two numbers bracketing the experimental result and each falling well within its uncertainty. The No. 2 value for ^{37}Cl is appreciably different

from that obtained in Ref. 3, however.

The calculations for ^{23}Na, ^{25}Mg, ^{27}Al, and ^{33}S presented in Ref. 2 were carried out in a variety of incomplete *sd*-shell model spaces and with a variety of complementary Hamiltonians and effective charge parametrizations. The minor differences between these results and the present predictions are thus unimportant. However, the results presented in Ref. 2 for ^{21}Ne, ^{35}Cl, and ^{37}Cl were obtained in the same full $d_{5/2}$-$s_{1/2}$-$d_{3/2}$ space used in Ref. 3 and the present work, and hence detailed comparisons again can highlight different configuration-mixing effects from different Hamiltonians. The quadrupole moment values obtained for ^{21}Ne and ^{35}Cl in Ref. 2 (with Hamiltonians from Refs. 40 and 41, respectively) are very similar to those obtained both in Ref. 3 and in the present work. The value obtained for ^{37}Cl is similar to the value obtained in the present work and thus also different from that obtained in Ref. 3.

2. *First-excited 2^+ states of doubly-even sd-shell nuclei*

The present results for static quadrupole moments of 2^+ first-excited states in doubly-even nuclei are quite similar to older[4] full-space results for $A=18$–28 which were based on the CWP Hamiltonian. The salient features, both of the present and the previous predictions and of the associated experimental values, are a small negative value for ^{18}O, large negative values for ^{20}Ne, ^{22}Ne, and ^{24}Mg, a smaller negative value for ^{26}Mg, and a large positive value for ^{28}Si. The values for ^{20}Ne, ^{22}Ne, and ^{24}Mg presumably reflect strong, stable prolate intrinsic states. In this same vein, the ^{26}Mg and ^{28}Si values reflect a rapid shape transition from prolate to oblate between $A=24$ and 28. The results for these nuclei presented in Ref. 2, obtained in truncated *sd*-shell spaces, are similar to the present and past results from calculations in full *sd*-shell spaces with the exception of ^{26}Mg. The two-orbit, $d_{5/2}$-$s_{1/2}$, wave functions used in Ref. 2 predicted a vanishing quadrupole moment. This result can be understood as a near complete cancellation in the $E2$ contribution coming from near-equal $(d_{5/2})^{10}$ and $(d_{5/2})^9$-$(s_{1/2})^1$ configurations. In the full-space results the $(d_{5/2})^{10}$ configuration dominates.

The present predictions for ^{30}Si, ^{32}S, ^{34}S, ^{36}Ar, and ^{38}Ar exhibit a variety of significant differences from the older results of Refs. 2 and 4; in addition, the older results also differ among themselves. Many of these variations can be understood as the consequences of the fact that the dominant configurations of most of these states, $(d_{3/2})^{2,J=2,T=1}$ or $(d_{3/2})^{4,J=2,T=0}$, yield vanishing matrix elements (the selection rule mentioned earlier) for the $E2$ operator. Hence, the predicted values of Q depend critically on smaller components of the wave functions.

The truncated-space results for ^{30}Si, ^{32}S, and ^{34}S of Ref. 2 should be inferior to full-space results of Ref. 3 and the present work in principle. The truncated-space result from Ref. 3 for ^{30}Si was -6.6 e fm^2, while the value obtained in Ref. 4 with the CWH Hamiltonian in the full space was $+9.9$ e fm^2 and the present value is $+2.9$ e fm^2. The present prediction for ^{32}S of about -10.5 e fm^2 agrees reasonably well with the current consensus for the experimental value. The truncated-space value from Ref. 2 of -14 e fm^2 is similar to the present value, but the CHW result in the full space[4] is much smaller in magnitude, -2.7 e fm^2. The present results for ^{34}S of about 4.2 e fm^2 are slightly smaller than the two, similar, older results, but not significantly different. There is also no significant difference between the new results and the older (full-space in both cases) values for ^{36}Ar.

B. Discussion of individual states

The theoretical values for the quadrupole moments of ^{17}O and ^{17}F are functions only of the assumptions made for the effective charges and the rms radii of the $d_{5/2}$ neutron and proton. The radii of the valence particle in $A=17$ are not directly measurable except via elastic magnetic electron scattering on ^{17}O. Measurements of the charge radius of ^{17}O are dominated by the radii of the p orbits, and there is no direct measurement of any sort for ^{17}F. The Saxon-Woods calculation is most appropriate for $A=17$. The fact that the calculated Saxon-Woods moment for ^{17}O is somewhat larger than experiment indicates either that the size of the valence radius is too large in the Saxon-Woods calculation or that the effective neutron charge is smaller than $0.45e$. The possible change in radius may be correlated with a similar problem for the magnetic form factor and the possible change in effective charge may be correlated with the expected state and binding-energy dependence of the effective charge.[14]

The predicted negative value of $Q(2_1^+,{}^{18}\mathrm{O})$, and hence the prolate shape of its intrinsic state in the context of the rotational model, is, as was discussed in Sec. II, a manifestation of strong mixing between the $(d_{5/2})^2$ (61%) and $(d_{5/2})^1$-$(s_{1/2})^1$ (32%) configurations. It is impossible within the *sd*-shell space to generate values of Q for this system which significantly exceed the present result. There is agreement between experiment and theory for ^{18}O, but the large experimental uncertainty precludes a quantitative comparison.

The predicted value of $Q(5_1^+,{}^{18}\mathrm{F})$ is, like the $A=17$ values, invariant to choice of Hamiltonian, since there is only one *sd*-shell configuration which can yield $J=5$ for two particles. The predicted value of $Q(\frac{5}{2}{}^+_1,{}^{19}\mathrm{F})$ is similar to the value for ^{17}F and also agrees within the uncertainty with experiment. This model wave function is dominated (48%) by the $(d_{5/2})^3$ configuration, with the $(d_{5/2})^1$-$(s_{1/2})^2$ (seniorities 1 and 3) configurations (11% and 6%) being next largest. Configuration mixing has a relatively small (20%) enhancement effect here on the value of Q. The proton matrix element $A(E2)_\mathrm{p}$ is close to the jj limit, $(d_{5/2})^3$, value while the neutron matrix element $A(E2)_\mathrm{n}$ is enhanced by a factor of 2.

The predicted value of $Q(2_1^+,{}^{20}\mathrm{F})$ also agrees with experiment within experimental uncertainty, completing the chain of agreement between theory and experiment for all four fluorine isotopes. The model wave function of this state is dominated (38%) by the $(d_{5/2})^4$ configuration with the $(d_{5/2})^3$-$(s_{1/2})^1$ configuration (12%) being the next largest. Configuration mixing increases the magnitude of both the neutron and proton matrix elements of this state over the jj-limit, $(d_{5/2})^4$, estimate and yields an enhancement of 2.5 in the value of Q.

The model wave function for ^{20}Ne(2_1^+) exhibits extensive configuration mixing. The largest probability (21%) component has a $(d_{5/2})^3$-$(s_{1/2})^1$ configuration and the second largest (14%) is $(d_{5/2})^4$. The value of Q is enhanced by a factor of 2.4 over the single component, $(d_{5/2})^3$-$(s_{1/2})^1$, estimate. The experimental value of Q is significantly larger than the predicted value. It is also significantly larger than the "dynamic moment" estimated from the measured $B(E2)$ of the $0_1^+ \rightarrow 2_1^+$ transition ($Q = -15.4 \pm 1.1$ e fm^2). This alternate experimental value only slightly exceeds the predicted value. In sum, the present shell-model wave function (and all previous ones) underestimate the quoted experimental value of the quadrupole moment of ^{20}Ne, but the significance of the underestimation is uncertain.

The predicted value of $Q(\frac{3}{2}_1^+, ^{21}\text{Ne})$ is in close agreement with the experimental value. This is to be contrasted with the just-noted ^{20}Ne result. The model wave function of this state is heavily configuration mixed, the component with the largest magnitude (19%) having the $(d_{5/2})^5$ configuration. The neutron and proton matrix elements of this $\Phi_i(NJT)$ are zero, so that the entire calculated value of Q is built up from "secondary" and "off-diagonal" contributions. The values of the neutron and proton matrix elements from configuration-mixed wave functions are nearly equal, so that the predicted value of Q for the ^{21}Na mirror state is only slightly larger than the ^{21}Ne value.

The predicted value of $Q(2_1^+, ^{22}\text{Ne})$ is similar to that of $Q(2_1^+, ^{20}\text{Ne})$. The quantitative differences are small enough that the various assumptions about the single-particle radial wave functions are an important issue. With the No. 2 calculations, in which the anomalously large r_{ch} of ^{20}Ne is manifest, the 10% decrease in going from ^{20}Ne to ^{22}Ne can be apportioned 5% to the decrease in r_{ch} and 5% to less coherent amplification of the proton matrix element from configuration mixing. Underlying the latter aspect is the fact that the configuration of the leading (19%) component of the model state, $(d_{5/2})^6$, has proton and neutron matrix elements of equal magnitude and opposite signs (a zero isoscalar value). The experimental value for ^{22}Ne, which is 20% smaller than that for ^{20}Ne, is still significantly larger than the predictions. Also, as was the case in ^{20}Ne, the analogous dynamic moment is smaller than the static moment, and close to the theoretical value. The combination of ^{20}Ne and ^{22}Ne results thus can be viewed in alternative contexts. In terms of the relative magnitudes, the experimental $Q(^{22}\text{Ne})/Q(^{20}\text{Ne})$ value of 0.83 ± 0.09 is consistent with the theoretical range of values which runs from 0.91 to 0.97. From another point of view, experiment and theory for ^{22}Ne are essentially consistent, within the experimental uncertainty, as opposed to the case of ^{20}Ne.

The experimental value of $Q(\frac{3}{2}_1^+, ^{23}\text{Na})$, measured with muonic atom techniques,[22] has an uncertainty (0.20 e fm^2, 2%) at least five times smaller than any of the preceding cases discussed except ^{17}O. The theoretical values No. 1, No. 2, and No. 3 are 3—6% (2—3 standard deviations) larger than experiment. In terms of the absolute and relative differences between predictions and measurement, the discrepancies are quite small. As in the case of the analogous wave functions for ^{21}Ne, the model wave function for ^{23}Na is strongly configuration mixed, with the leading component (16%) being $(d_{5/2})^7$. Also as in the case of ^{21}Ne, this component has neutron and proton matrix elements which are zero, so that all contributions to the net value of the configuration-mixed matrix element involve the smaller components of the wave function. Finally, again in parallel with $A = 21$, the configuration-mixed proton and neutron matrix elements for this wave function are very nearly equal, that is, the "isovector" matrix element is nearly zero.

The model wave function for ^{24}Mg(2_1^+) has for its largest (14%) component the $(d_{5/2})^8$ configuration. This component yields neutron and proton $E2$ matrix elements whose values are smaller than those of the $(d_{5/2})^3$-$(s_{1/2})^1$ component which is the leading term in the ^{20}Ne(2_1^+) model wave function. The coherent amplification from configuration mixing is 20% greater than was obtained in ^{20}Ne and yields a factor of 4 enhancement of Q over the jj-limit, $(d_{5/2})^8$, value. The theoretical values of $Q(2_1^+, ^{24}\text{Mg})$ are 1—2 e fm^2 (5—10%) smaller than the experimental value, but lie within its estimated uncertainty.

The experimental value of $Q(\frac{5}{2}_1^+, ^{25}\text{Mg})$ has also been obtained with the muonic-atom technique[23] and has an uncertainty of 1.5% (0.3 e fm^2). Again, this is an order of magnitude better than the typical uncertainties in experimental values which we must deal with. In this case, the predictions (No. 1, No. 2, and No. 3) are 3—7% (2—3 standard deviations) *smaller* than the experimental value, rather than larger as in the case of ^{23}Na. Again, the discrepancies are, in context, both absolutely and relatively small.

The largest component (21%) in the model wave function for ^{25}Mg($\frac{5}{2}_1^+$) is $(d_{5/2})^9$. The configuration-mixed value of Q is enhanced by a factor of 2.8 over the value of this pure-jj component. Unlike the case of ^{21}Ne and ^{23}Na, the configuration-mixed proton matrix element $A(E2)_{\text{p}}$ for ^{25}Mg is larger than the neutron matrix element $A(E2)_{\text{n}}$. Hence, the value of $Q(\frac{5}{2}_1^+, ^{25}\text{Al})$ is predicted to be smaller than that of the mirror ^{25}Mg state, in spite of ^{25}Al having one additional proton. This effect can be understood from the point of view of the effective number of holes in the $d_{5/2}$ orbit and their ability to participate in configuration mixing. With a single $d_{5/2}$ neutron hole, but two $d_{5/2}$ proton holes, ^{25}Mg accommodates more coherent amplification from mixing among proton configurations than from among neutron configurations, this situation reversing in the mirror system.

The leading component (17%) of the model wave function for ^{26}Mg(2_1^+) is $(d_{5/2})^{10}$. This term is the proton-hole analog of the $(d_{5/2})^2$ neutron component of the ^{18}O wave function. With the jj-limit wave function, ^{26}Mg would have a quadrupole moment of the same magnitude (except for scaling for the radial wave function size), but opposite in sign, to that of ^{18}Ne, the mirror state of ^{18}O. The configuration mixing predicted for ^{26}Mg is, however, completely different from that calculated for ^{18}O—^{18}Ne. The predicted value of Q is enhanced by a factor of 2.4 over the $(d_{5/2})^{-2}$ estimate by the effects of configuration mixing. As in the case of ^{25}Mg-^{25}Al, the predicted magnitude of $Q(2_1^+, ^{26}\text{Mg})$ is predicted to be larger than that of

$Q(2_1^+,{}^{26}\mathrm{Si})$. The theoretical values for ^{26}Mg agree with experiment comfortably within the experimental uncertainties. The observed decrease in the experimental moment of ^{26}Mg relative to that of ^{24}Mg is accurately reproduced by the model results.

The model wave function for $^{27}\mathrm{Al}(\frac{5}{2}_1^+)$ is dominated (26%) by the "single hole" $(d_{5/2})^{11}$ configuration, with "three-hole–two-particle" $(d_{5/2})^9$-$(s_{1/2})^2$ configurations accounting for another 15%. Configuration mixing enhances the proton matrix element $(AE2)_p$ by a factor of 1.5 and creates a significant neutron matrix element $(AE2)_n$ as well. The overall enhancement of the value of Q over the *jj*-limit estimate is 1.7. This nucleus is the third and last in the *sd* shell for which a muonic-atom experiment has been carried out.[23] The experimental uncertainty in this case is appreciably larger than for ^{23}Na or ^{25}Mg, but the new measurement still represents a significant improvement over the previous situation. The predictions No. 2 and No. 3 agree with the experimental value to well within the uncertainty, while prediction No. 1 is one standard deviation larger.

The model wave function for $^{28}\mathrm{Si}(2_1^+)$ is dominated (12%) by the one-hole–one-particle $(d_{5/2})^{11}$-$(s_{1/2})^1$ configuration, followed by a variety of three-hole–three-particle components. All of these components yield signs for the value of the one-body densities and the $E2$ matrix elements which are opposite to those obtained for ^{20}Ne, ^{22}Ne, ^{24}Mg, and ^{26}Mg. In the language of the collective rotational model, the model wave function for ^{28}Si has emerged with an oblate deformation rather than the prolate shapes which characterized the lighter even-even systems. The enhancement of the configuration-mixed value of Q over the *jj*-limit, $(d_{5/2})^{11}$-$(s_{1/2})^1$, value is a factor of 3.8. The three predictions No. 1, No. 2, and No. 3 are all essentially equal, and are slightly larger than the experimental estimate, although well within its uncertainty.

The model wave function for $^{30}\mathrm{Si}(2_1^+)$ is significantly different from the wave functions for smaller A values. The configuration of the leading (25%) component, $(d_{5/2})^{12}$-$(s_{1/2})^1$-$(d_{3/2})^1$, reflects the "shell effects" of both the approximate "filling" of the $d_{5/2}$ subshell at $A=28$ and the impossibility of forming a $J=2$ state within the confines of the next, $j=\frac{1}{2}$, subshell. The next most important components have $(d_{5/2})^{11}$-$(s_{1/2})^3$ (9%), $(d_{5/2})^{11}$-$(s_{1/2})^1$-$(d_{3/2})^2$ (7%), etc., configurations. Configuration mixing results in a competition between the "particle" (neutron) nature of the leading component and the "hole" nature of the admixed components.

The dominant neutron one-body density is the $D^{NJTT_z}(2,\frac{3}{2},\frac{3}{2})$ term, whose positive (corresponding to "prolate" shape) value comes from the leading component, overcoming smaller canceling contributions from admixed terms. The net neutron matrix element $A(E2)_n$ is reduced by a factor of 0.44 from this *jj*-limit, $(d_{3/2})^1$-$(s_{1/2})^1$, estimate by configuration mixing. The proton matrix element of the leading $(d_{3/2})^1$-$(s_{1/2})^1$, component of $^{30}\mathrm{Si}(2_1^+)$ is zero. Nonetheless, configuration mixing generates a net proton matrix element $A(E2)_p$ which is larger than the neutron matrix element $A(E2)_n$. Moreover, the neutron and proton contributions have opposite signs. When weighted by the values of the effective neutron and proton charges, the net value for Q is small and positive, $+3$ $e\,\mathrm{fm}^2$, reflecting the slight dominance of proton configuration mixing over the contribution of the simple, two-neutron component.

The single experimental value is small and negative, -5 $e\,\mathrm{fm}^2$, with an uncertainty of 6 $e\,\mathrm{fm}^2$. Hence, there is not a significant contradiction of the present predication by experiment in spite of the opposite signs. The shell-model result is obviously extremely sensitive to the specific individual details of configuration mixing, both as this affects the attenuation of the neutron matrix element and as it affects the cancellation between neutron and proton contributions.

The model wave function for $^{32}\mathrm{S}(2_1^+)$ has for its leading components the $(d_{5/2})^{12}$-$(s_{1/2})^3$-$(d_{3/2})^1$ (21%) and $(d_{5/2})^{12}$-$(s_{1/2})^1$-$(d_{3/2})^3$ (15%) configurations. Configurations with $d_{5/2}$-hole structure have individual probabilities of 5% or less. This dominant "particle-like" structure is reflected in the positive values of the one-body-transition densities, the largest terms of which are $D^{NJTT_z}(2,\frac{1}{2},\frac{3}{2})$ and $D^{NJTT_z}(2,\frac{3}{2},\frac{3}{2})$. The predicted value of $Q(2_1^+,{}^{32}\mathrm{S})$ is definitely prolate and is enhanced by a factor of 2.6 over the value of the *jj*-limit configuration $(s_{1/2})^3$-$(d_{3/2})^1$.

The present wave functions for ^{32}S and ^{30}Si exhibit somewhat more configuration mixing from the $d_{5/2}$ to the $s_{1/2}$-$d_{3/2}$ subspace than the first[2] truncated-space results for these nuclei, but less than the full-space CWH wave functions used in Ref. 4. Hence the present values of Q are less negative than those of Ref. 2 and more negative than those of Ref. 4, remembering that the leading $s_{1/2}$-$d_{3/2}$ components of both systems yield a negative value of Q while the components featuring $d_{5/2}$ holes typically yield positive values. The history of the experimental value of $Q(2_1^+,{}^{32}\mathrm{S})$ is somewhat confused by the occurrence at an intermediate point in time of an anomalously small value. Earlier and later work suggests a negative value which is somewhat larger than the present predictions. The predicted values are only about half those found for the lighter nuclei ^{20}Ne, ^{22}Ne, ^{24}Mg, and ^{28}Si.

The dominant (42%) component in the model wave function for ^{33}S is $(d_{3/2})^1$. The next most important configurations have 2p-2h structure relative to this leading term and hence do not connect with it via one-body operators. The net neutron matrix element $A(E2)_n$ hence is only slightly (15%) enhanced by configuration mixing. The value of $A(E2)_p$, on the other hand, is boosted from zero to a value 50% as large as $A(E2)_n$ by configuration mixing. Hence, when weighted by effective charges, the predicted value of Q has a larger "proton" than "neutron" contribution. The predicted values are comfortably within the quoted uncertainty of the experimental value.

The leading component (25%) in the model wave function for $^{34}\mathrm{S}(2_1^+)$ is $(d_{5/2})^{12}$-$(s_{1/2})^4$-$(d_{3/2})^2$, which via the selection rule noted earlier has a zero quadrupole matrix element. The next most important wave function components have the $(s_{1/2})^3$-$(d_{3/2})^3$ configuration, one (13%) corresponding to the $T=\frac{3}{2}$ coupling of $(d_{3/2})^3$ and the other (11%) to the $T=\frac{1}{2}$ coupling. The $T=\frac{3}{2}$ coupling for ^{34}S corresponds to a positive, neutron-only contribu-

tion to the $E2$ matrix element, while the $T=\frac{1}{2}$ coupling yields significant negative contributions in both the neutron and proton channels. The most important one-body-transition density is the off-diagonal $D^{NJTT_z}(2,\frac{1}{2},\frac{3}{2})$ term. Its contribution to the net neutron matrix element $A(E2)_n$ is reinforced by the other $D^{NJTT_z}(2,\rho,\rho')$ terms, so that the resultant value is almost comparable to the typical "large" neutron terms in other systems. The net proton matrix element $A(E2)_p$, however, is quite small, the consequence of an almost complete cancellation between the diagonal ρ-$\rho'=\frac{3}{2}$-$\frac{3}{2}$ contribution from the $(d_{3/2})^{3,T=1/2}$ component in the wave function and "background" contributions of the opposite sign. The predicted value of $Q(2_1^+,{}^{34}\mathrm{S})$ thus is more than normally dependent upon the neutron component of the wave function. The small positive predicted values lie well within the uncertainties of the experimental value.

The model wave functions of $^{35}\mathrm{Cl}(\frac{3}{2}_1^+)$ and $^{35}\mathrm{S}(\frac{3}{2}_1^+)$ are dominated, respectively, by the $(d_{3/2})^{3,T=1/2}$ (54%) and $(d_{3/2})^{3,T=3/2}$ (78%) configurations. Configuration mixing enhances the jj'-limit estimates of the values of Q by a factor of 1.4 for ^{35}Cl and a factor of 2.4 for ^{35}S. The principal effect of mixing for ^{35}Cl is to enhance the neutron matrix element more than the proton and thus make the net value of Q more "isoscalar" (neutron and proton matrix elements almost equal).

The leading component (88%) in the model wave function of $^{36}\mathrm{S}(2_1^+)$ is $(s_{1/2})^3$-$(d_{3/2})^5$. The neutron components are identically zero since, with the assumption of a $d_{5/2}$-$s_{1/2}$-$d_{3/2}$ basis space, $N=20$ corresponds to totally filled, and therefore inert, neutron shells. The model wave function for the 2^+ ground state of ^{36}Cl has as its leading component (84%) the $(d_{3/2})^4$ configuration, with the $(d_{5/2})^{10}$-$(s_{1/2})^4$-$(d_{3/2})^6$ configuration as the second largest contribution, comprising about 4% of the complete wave function. In the pure jj'-limit $(d_{3/2})^4$ configuration, the value of the quadrupole moment is identically zero due to the selection rule mentioned earlier. It is therefore unsurprising that the configuration-mixed wave function dominated (84%) by the $(d_{3/2})^4$ configuration should lead to a small vlaue of the $E2$ matrix element or quadrupole moment and that the calculated value is very sensitive to the details of the Hamiltonian. The experimental value of $Q(2_1^+;{}^{36}\mathrm{Cl})$, at $-1.8\ e\,\mathrm{fm}^2$, is one of the smallest measured in the sd-shell region. The calculated value of $Q(2_1^+;{}^{36}\mathrm{Cl})$ is smaller in magnitude than the experimental result by a factor of 5 and, moreover, has the opposite sign. The previously studied Hamiltonians[2,3] yield values of -0.9 and $-2.7\ e\,\mathrm{fm}^2$, respectively.

The leading component (34%) in the model wave function of $^{36}\mathrm{Ar}(2_1^+)$ is $(d_{3/2})^4$, with the second largest component being $(s_{1/2})^3$-$(d_{3/2})^{5,T=1/2}$ (20%). The $(d_{3/2})^4$ configuration yields a zero $E2$ matrix element. The off-diagonal contributions between these two leading terms have the same sign as the diagonal contribution from the $(s_{1/2})^3$-$(d_{3/2})^3$ component. The resultant values predicted for $Q(2_1^+,{}^{36}\mathrm{Ar})$ are positive, agreeing in sign and magnitude with the only existing experimental value.

As was the case for ^{36}S, only proton configurations are active in the model wave functions for $^{37}\mathrm{Cl}(\frac{3}{2}_1^+)$. The leading component is $(d_{3/2})^5$, with a 93% probability. The extreme simplicity of this wave function relative to almost all of the others we have discussed highlights two general features. One is the sensitivity of the results to configuration mixing, the other is the difficulty of distinguishing "neutron" from "proton" contributions unambiguously in typical cases.

As is evident from the $A(E2)$ entries in Table I, the model wave functions predict a dominant "isoscalar" character for most of the states considered, namely, the values of the "neutron" and "proton" matrix elements $A(E2)_{n/p}$ are comparable in size. This, in turn, makes it essentially impossible to use theoretical-experimental comparisons within this data set to establish an empirically optimum "isovector" $(\tilde{e}_p-\tilde{e}_n)$ effective charge. If both matrix elements are equal, than the net moment values are essentially invariant to any choice of $\tilde{e}_p$ and $\tilde{e}_n$, which leaves the $\tilde{e}_p+\tilde{e}_n$ sum invariant. Only for the oxygen isotopes and the $N=20$ isotones do we have the opportunity to view (in the model context) only neutrons or only protons. The issue for neutrons is clouded by uncertainties about the correct radial wave functions for ^{17}O and the small value for the ^{18}O moment, which entails both model and experimental uncertainties.

These problems should not exist for ^{37}Cl. The appropriate value for the radius is known and the wave function is simple in the model context. A comparison of theory with experiment should yield unambiguous information about the optimum value of $\tilde{e}_p$. Inspection of the ^{37}Cl entries in Table III reveals a clear difference between the harmonic-oscillator, $\tilde{e}_p\approx 1.35e,\tilde{e}_n\approx 0.35e$ results and the Saxon-Woods, $\tilde{e}_p\approx 1.15e,\tilde{e}_n\approx 0.45e$ results. The $\tilde{e}_p\approx 1.15e,\tilde{e}_n\approx 0.45e$ results are in better agreement with experiment. This is not a radial wave function effect since, as was noted earlier, the radii of the active orbits for this region of the shell are almost identical in each prescription. Likewise, since the ^{35}Cl and ^{37}Cl data are measured together, the *ratio* of the two values is very accurately known, since the Sternheimer corrections should be nearly identical for the two isotopes.

We conclude that this ^{37}Cl datum is significant additional evidence for the empirical determination of the optimum combination of radial wave functions and effective charges with which to treat isovector $E2$ phenomena. However, it is appropriate to add a cautionary note, apropos the sensitivity of the value of Q to configuration mixing effects even in this apparently simple case. As was noted earlier, the predictions of Ref. 2 for $Q(^{37}\mathrm{Cl})/Q(^{35}\mathrm{Cl})$ were similar to the present results No. 1 and No. 2, while the predictions of Ref. 3, which are also analogous to the present results No. 1 and No. 2 in so far as radial wave functions (harmonic oscillator) and effective charges $\tilde{e}_p\approx 1.35e,\tilde{e}_n\approx 0.35e$ are concerned, show a ratio $Q(^{37}\mathrm{Cl})/Q(^{35}\mathrm{Cl})$ which is in agreement with the experimental decrease, hence inconsistent with the present No. 1 and No. 2 predictions.

Inspection of the one-body-density matrix elements in Table I of Ref. 3 and in Table I of the present work shows that the difference in the values of Q for $^{37}\mathrm{Cl}(\frac{3}{2}_1^+)$ results from a different magnitude and sign of the $D^{NJTT_z}(2,\frac{1}{2},\frac{3}{2})$ element. (Equation 14 of Ref. 12 gives

the relationship between the proton-neutron representation for the one-body-transition densities presented in Table I of this work and the isoscalar-isovector representation presented for the one-body-transition densities in Table I of Ref. 3.) The $s_{1/2}$-$d_{3/2}$ one-body-transition density term is small and positive in Table I here while considerably smaller still in magnitude, and negative, in Ref. 3. The three Hamiltonians used to obtain the ^{37}Cl quadrupole moments in Ref. 2, Ref. 3, and the present work give probabilities for the dominant $(d_{3/2})^{-3}$ configuration in the wave function of $^{37}\mathrm{Cl}(\frac{3}{2}^+_1)$ which are 91%, 92%, and 93%, respectively. The second most heavily weighted configuration in each of these wave functions is $(d_{5/2})^{-2}$-$(d_{3/2})^{-1}$, with probabilities of 3.5%, 4.2%, and 1.7%, respectively. This configuration does not connect with the dominant configuration through a one-body operator, so it makes a negligible contribution to the quadrupole moment.

The operative configuration in explaining the difference between the results of Ref. 3 on one hand and of Ref. 2 and the present calculation on the other is $(s_{1/2})^{-1}$-$(d_{3/2})^{-2}$. It has probabilities of 0.9%, 0.07%, and 1.25%, respectively, in the wave functions of Ref. 2, Ref. 3, and Ref. 6. The key to the different results for Q, however, is that this configuration and the dominant $(d_{3/2})^{-3}$ configuration have amplitudes with the same relative sign in the wave function of Ref. 3 and with opposite signs in the wave function of Refs. 2 and 6. Hence, the change of 20% in the predicted quadrupole moment of $^{37}\mathrm{Cl}(\frac{3}{2}^+_1)$ between Ref. 3 and the No. 2 prediction of the present work results from the change of relative sign in a 1% component in the wave function.

Confirming evidence for the correctness of the $\tilde{e}_p \approx 1.15e, \tilde{e}_n \approx 0.45e$ choice comes from the case of ^{39}K. In the present model this quadrupole moment is strictly a measure of the radial wave function and proton effective charge. Again, the choice of radial wave functions is not a significant factor in differentiating between the various net results. The experimental value clearly favors $\tilde{e}_p \approx 1.15e$. The quadrupole moment of the remaining $N=20$ isotone, ^{38}Ar, is unmeasured. Its predicted value again illustrates the great sensitivity of Q which can occur from small admixtures in the model wave function.

The present wave function for $^{38}\mathrm{Ar}(2^+_1)$ is dominated (93%) by $(d_{3/2})^{-2}$. Due to the selection rule previously mentioned, this configuration has a zero $E2$ matrix element, which explains the small value for the $D^{NJTT_z}(2,\frac{3}{2},\frac{3}{2})$ one-body density in Table I. Because of the dominance of the $(d_{3/2})^{-2}$ component, the only paths to generating appreciable one-body-density values are the connections of the $(d_{5/2})^{-1}$-$(d_{3/2})^{-1}$ and $(s_{1/2})^{-1}$-$(d_{3/2})^{-1}$ components to the $(d_{3/2})^{-2}$ component. The contributions will be essentially proportional to the amplitudes of these two small components. In the present calculation the $(s_{1/2})^{-1}$-$(d_{3/2})^{-1}$ component has a 5% probability and the remaining components each less than 1%. In the $^{38}\mathrm{Ar}(2^+_1)$ wave function of Ref. 2, the probability of $(d_{3/2})^{-2}$ is 94% and that of $(s_{1/2})^{-1}$-$(d_{3/2})^{-1}$ is 2% and the value of Q is only half that of the present prediction. In the CWH wave function, the $(d_{3/2})^{-2}$ component probability is 98.5%, and the $(s_{1/2})^{-1}$-$(d_{3/2})^{-1}$ probability is 0.24% and has a sign relative to the $(d_{3/2})^{-2}$ component which is opposite to that found in the other two wave functions. Its effect is thus aligned with that of the $(d_{5/2})^{-1}$-$(d_{3/2})^{-1}$ contribution and a very small negative value of Q emerges for ^{38}Ar in Ref. 4.

The difference between the present and past calculations for the ^{36}Cl, ^{37}Cl, and ^{38}Ar moments appears to be traceable to the

$$\langle d_{3/2}d_{3/2} \mid V \mid d_{3/2}s_{1/2} \rangle$$

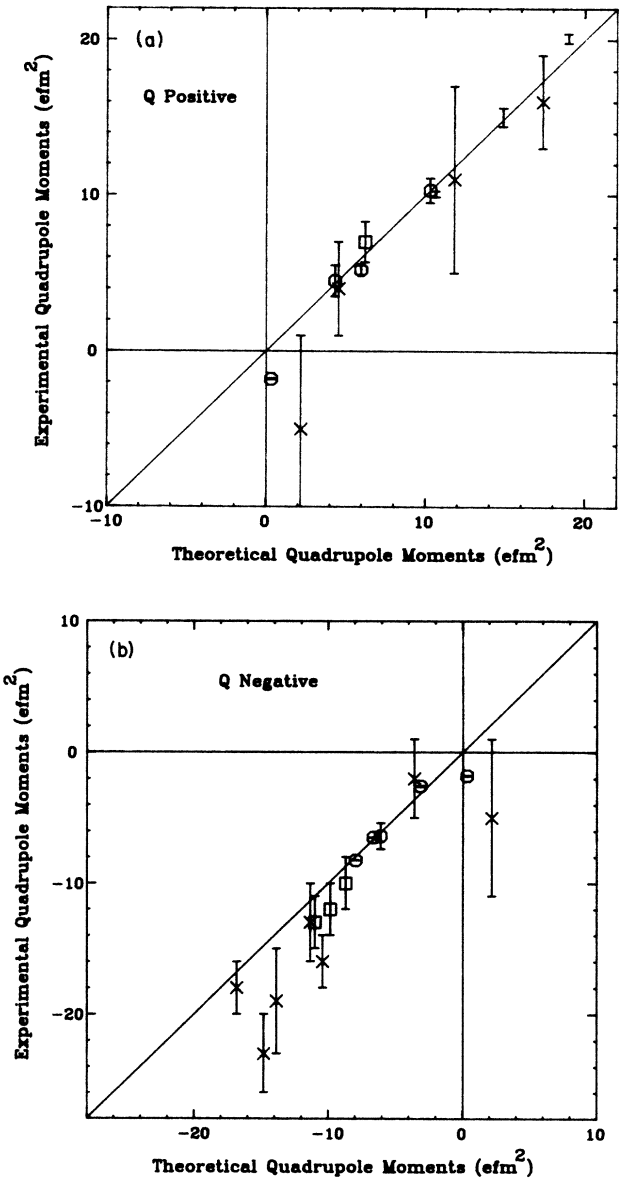

FIG. 2. (a) Comparison of measured and predicted (calculation No. 3) electric quadrupole moments of *sd*-shell states which have *positive* values. The octagons correspond to the electronic-atom measurements, the $\times$'s correspond to the quadrupole moments of the 2^+_1 excited states, the boxes correspond to the quadrupole moments of the fluorine isotopes and the plain vertical bars correspond to the muonic-atom measurements. (b) Comparison of measured and predicted (calculation No. 3) electric quadrupole moments of *sd*-shell states which have *negative* values. The notation is as in (a).

two-body matrix elements of the effective Hamiltonian. These off-diagonal matrix elements are very poorly determined in the context of eigenvalue-level energy comparisons, and the present type of study offers perhaps the best path towards determining their correct values.

V. SUMMARY AND CONCLUSIONS

A systematic shell-model formulation of static electric quadrupole moments of *sd*-shell states [summarized in Figs. 2(a) and 2(b)] has been shown here to yield a comprehensive accounting of experimental values. The formulation incorporates the configuration-mixed wave functions from a complete and unified shell-model calculation for *sd*-shell nuclei, radial wave functions alternatively of the harmonic-oscillator and Saxon-Woods forms, each with radial scales set to reproduce measured rms radii, and mass-independent, state-independent effective charges for the protons and neutrons active in the model wave functions, the values of the charges being matched to the two types of radial wave functions. The results from different radial wave function—effective charge prescriptions typically were insignificantly different from each other. From the cases for which there were significant differences (principally for model states with either pure proton or pure neutron wave functions) there emerged evidence that the Saxon-Woods prescription, more particularly, the $\tilde{e}_p = 1.15e, \tilde{e}_n = 0.45e$ values of the effective charges associated with it, are to be preferred. This choice is necessary in particular to account for the $Q(^{37}\mathrm{Cl})/Q(^{35}\mathrm{Cl})$ ratio and the value of the ^{39}K moment.

The calculated values of electric quadrupole moments are sensitive functions of configuration mixing in the shell-model wave functions. The larger-magnitude calculated moments correspond to factors of 2 to 4 enhancements over the values predicted from simple, one-component, *jj*-coupling wave functions. In the cases of some small-magnitude moments, the calculated values from the configuration-mixed wave functions even differ in sign from the simple estimates. The overall trends of the quadrupole moment data, which are distributed over values from -20 to $+20$ e fm^2 as a complex function of N and Z, are well reproduced by the one-body densities from the configuration-mixed wave functions in conjunction with constant effective charge models. The single-particle values of ^{17}O, ^{17}F, ^{18}F, and ^{39}K connect smoothly with the many-particle values, both large and small, which are generated out of the mixing in wave functions with hundreds or even thousands of components.

Systematic features to note include the progression of moment ratios for the fluorine isotopes, $Q(^{18}\mathrm{F})/Q(^{17}\mathrm{F}) = +1.33 \pm 0.08$ (experiment) vs $+1.26$ (No. 3), $Q(^{19}\mathrm{F})/Q(^{17}\mathrm{F}) = +1.24 \pm 0.06$ (experiment) vs $+1.13$ (No. 3), and $Q(^{20}\mathrm{F})/Q(^{17}\mathrm{F}) = -0.70 \pm 0.02$ (experiment) vs -0.71 (No. 3), and the chlorine isotopes $Q(^{37}\mathrm{Cl})/Q(^{35}\mathrm{Cl}) = +0.79$ (experiment) vs $+0.78$ (No. 3). Another noteworthy point is the excellent agreement between theory and the three values determined in muonic-atom measurements (^{23}Na, ^{25}Mg, ^{27}Al). The predictions for the "true" single $d_{5/2}$ proton state in ^{17}F and the "quasi"-single $d_{5/2}$ proton hole state in ^{27}Al differ by a factor of 2, in rough agreement with experiment. The predictions for the quasi-single $d_{3/2}$ neutron state in ^{33}S agree with experiment and are likewise about twice as large in magnitude as predicted for the "true" single $d_{3/2}$ neutron hole state in ^{39}Ca.

The detailed features of the observed region of strong prolate deformation extending from ^{20}Ne through ^{21}Ne, ^{22}Ne, ^{23}Na, ^{24}Mg, ^{25}Mg, to ^{26}Mg are well reproduced theoretically with the exception of the magnitudes of the ^{20}Ne and, to a lesser degree, ^{22}Ne moments. The large experimental values for these two states may reflect problems in the reorientation-effect experiments. The sharp transition to oblate deformation at ^{28}Si is unambiguously predicted by these shell-model wave functions, as is the rapid transition back to prolate at ^{32}S, passing through the small value of the ^{30}Si moment. The sign of the ^{30}Si moment is incorrectly predicted. The experimental value has a large uncertainty and the shell-model prediction is very sensitive to small details in the configuration mixing. The magnitudes of the predicted moment ^{32}S are also quite sensitive to configuration mixing details. The present value is appreciably smaller than the experimental value quoted here, although in agreement with the value quoted in Ref. 29. Finally, the predicted change from a "large" negative moment to a "small" positive moment in going from ^{32}S to ^{34}S is in agreement with the available experimental evidence.

We would conclude that more precise and more extensive measurements of static quadrupole moments are necessary to extend the tests of theory, either of the configuration mixing from shell-model Hamiltonians or the details of the renormalizations of the $E2$ operator, beyond the stage reached in this study.

ACKNOWLEDGMENTS

Informative discussions with Dirk Schwalm and Wilton Chung are gratefully acknowledged. This work was supported in part by National Science Foundation Grants No. 85-09736 and No. 83-12245.

[1] P. Brix, Z. Naturforsch. **41a**, 3 (1986).
[2] B. H. Wildenthal, J. B. McGrory, and P. W. M. Glaudemans, Phys. Rev. Lett. **26**, 96 (1971).
[3] B. A. Brown, W. Chung, and B. H. Wildenthal, Phys. Rev. C **22**, 774 (1980).
[4] B. H. Wildenthal, Nucleonika **23**, 459 (1978).
[5] G. A. Timmer, F. Meurders, P. J. Brussaard, and J. F. A. van Hienen, Z. Phys. A **288**, 83 (1978).
[6] B. H. Wildenthal, Prog. Part. Nucl. Phys. **11**, 5 (1984).
[7] B. A. Brown and B. H. Wildenthal, Phys. Rev. C **28**, 2397 (1983).
[8] B. A. Brown and B. H. Wildenthal, At. Data Nucl. Data

Tables **33**, 347 (1985).
[9]B. A. Brown, R. Radhi, and B. H. Wildenthal, Phys. Rep. **101**, 313 (1983).
[10]P. J. Brussaard and P. W. M. Glaudemans, *Shell-Model Applications in Nuclear Spectroscopy* (North-Holland, Amsterdam, 1977).
[11]G. F. Bertsch, *The Practitioner's Shell Model* (North-Holland, Amsterdam, 1972).
[12]J. L. Friar and J. W. Negele, *Advances in Nuclear Physics,* edited by M. Baranger and E. Vogt (Plenum, New York, 1975), Vol. 8, p. 219.
[13]B. A. Brown *et al.*, Phys. Rev. C **26**, 2247 (1982).
[14]B. A. Brown, A. Arima, and J. B. McGrory, Nucl. Phys. **A277**, 77 (1977).
[15]H. Sagawa and B. A. Brown, Nucl. Phys. **A430**, 84 (1984).
[16]T. K. Alexander, B. Castel, and I. S. Towner, Nucl. Phys. **A445**, 189 (1985).
[17]R. D. Lawson, *Theory of the Nuclear Shell Model* (Clarendon, Oxford, 1980).
[18]*Table of Isotopes,* 7th ed., edited by C. Michael Lederer and Virginia S. Shirley (Wiley, New York, 1978).
[19]R. M. Sternheimer, Phys. Rev. **86**, 316 (1952).
[20]R. M. Sternheimer and R. F. Peierls, Phys. Rev. A **4**, 1722 (1971).
[21]M. Elbel and R. Quad, Z. Naturforsch. **41a**, 15 (1986).
[22]B. Jeckelmann *et al.*, Nucl. Phys. **A408**, 495 (1983).
[23]R. Weber *et al.*, Nucl. Phys. **A377**, 361 (1982).
[24]T. Minamisono, Y. Nojiri, A. Mizobuchi, and K. Sugimato, Nucl. Phys. **A234**, 416 (1974).
[25]Kenzo Sugimato, Akira Mizobuchi, and Kozi Nazai, Phys. Rev. **134**, B539 (1964).
[26]H.-J. Stöckmann *et al.*, Z. Phys. **269**, 47 (1974).
[27]H. Enteneuer *et al.*, Phys. Rev. C **16**, 1703 (1977).
[28]J. de Boer and J. Eichler, *Advances in Nuclear Physics,* edited by M. Baranger and E. Vogt (Plenum, New York, 1968), Vol. 1, p. 1.
[29]R. H. Spear, Phys. Rep. **73**, 369 (1981).
[30]D. Schwalm *et al.*, Nucl. Phys. **A192**, 449 (1972).
[31]D. Schwalm, E. K. Warburton, and J. W. Olness, Nucl. Phys. **A293**, 425 (1977).
[32]R. H. Spear *et al.*, Nucl. Phys. **A378**, 559 (1982).
[33]M. P. Fewell *et al.*, Phys. Rev. Lett. **43**, 1463 (1979).
[34]G. C. Ball *et al.*, Nucl. Phys. **A349**, 271 (1980).
[35]G. Dannhauser *et al.*, Z. Phys. A **300**, 71 (1981).
[36]W. J. Vermeer, M. T. Esat, and R. H. Spear, Nucl. Phys. **A389**, 185 (1982).
[37]K. Nakai, F. S. Stephens, and R. M. Diamond, Phys. Lett. **34B**, 389 (1971).
[38]H. Clement *et al.*, Phys. Rev. Lett. **45**, 599 (1980).
[39]W. Chung, Ph.D. thesis, Michigan State University, 1976.
[40]B. M. Preedom and B. H. Wildenthal, Phys. Rev. C **6**, 1633 (1972).
[41]B. H. Wildenthal, E. C. Halbert, J. B. McGrory, and T. T. S. Kuo, Phys. Rev. C **4**, 1266 (1971).